



Research paper

# Hydroelastic response of Froude scaled stiffened steel panels exposed to design-critical wave slamming

Bjørn Christian Abrahamsen<sup>a,\*</sup>, Frode Grytten<sup>b</sup>, Erik Andreassen<sup>b</sup>, Øyvind Hellan<sup>a</sup>

<sup>a</sup> SINTEF Ocean, Jonsvannsveien 82, Trondheim 7050, Norway

<sup>b</sup> Department Materials and Nanotechnology, SINTEF Industry, Pb. 124 Blindern, Oslo 0314, Norway

## ARTICLE INFO

### Keywords:

Wave impact load  
Hydroelasticity  
Fluid structure interaction  
Extreme value statistics  
Model test  
3D printing  
Froude scaling

## ABSTRACT

Stiffened steel panels of offshore ocean structures may experience violent wave impacts which needs to be accounted for in design. The slamming pressures are often measured in scaled wave tank tests and imposed on finite element models to obtain local structural responses. These responses are sometimes high, which has raised the question if hydroelastic effects are properly accounted for. One way to address the uncertainty of hydroelasticity, is to carry out hydroelastic model tests and compare measurements statistically with FEA calculations. This paper presents the hydroelastic model tests required for this type of comparison. Approximate elastic panels representing Froude scaled stiffened steel panels were 3D printed, validated, and then installed in a vertical column in a wave tank. The elastic panels were exposed to design critical wave slamming during irregular wave conditions relevant for the North Atlantic. Two different elastic panels were tested, one strong and one weak panel. The hydroelastic response of the elastic panels are reported in detail and shows that the panel responds with a limited set of frequencies. In most cases the strain time series of the stiffeners and girders obtain its maximum value during the first half period of vibration. Furthermore, the vibration of the panels generally show strong decay after the time of maximum strain. The extreme strains fit reasonably well with the Gumbel distribution. Furthermore, the variability of the extreme strains, measured as the coefficient of variation (COV), is comparable to the variability of slamming pressures from literature, for the strong elastic panel, but is found to be reduced significantly for the weak elastic panel.

## 1. Introduction

Stiffened steel panels are fundamental structural components in ships and ocean structures. A critical design parameter is impact loads from steep and energetic waves. Design of such panels are typically done in two steps: first establishing the relevant wave slamming loads, and then calculating the structural response. The wave slamming loads are typically measured during Froude-scaled model tests carried out in wave tanks or ocean basins. The structural response is calculated using static or dynamic finite element analyses (FEA). This type of response analysis based on measured wave impact pressures is referred to as the design procedure in this paper. This procedure has been debated during recent revisions of rules and regulations for mobile offshore units (DNV-OTG-14, 2019). Operators claim calculated structural responses (damages) are over-estimated compared to reported damages from mobile offshore units in operation. The question is whether this procedure is accurate, and what uncertainties are inherent in the design

procedure which could explain potential conservatism.

The main uncertainties of such a design procedure are; (1) the accuracy of the slamming force measurements, (2) the scaling of slamming loads, (3) the statistical variation of measured slamming loads and (4) the load modifications due to structural deformations, i.e. the hydroelastic effects.

The primary objective of the present work is to study hydroelastic response of orthogonally stiffened panels in a Froude scaled model experiment at a scale of 1:40. A vertical surface-piercing column is exposed to several realisations of a design-critical three-hour sea-state. We have considered a three-hour sea-state that is relevant for survival limit state design, e.g. NORSOK standard N-003 (2017), i.e., metocean conditions with annual exceedance probability of  $10^{-2}$ , and which has been identified as design critical in terms of slamming loads. This sea-state is repeated many times to determine the distribution function for (three-hour) extreme structural response. The structural response is measured on an elastic panel located where the highest impact loads are

\* Corresponding author.

E-mail address: [bjornchristian.abrahamsen@sintef.no](mailto:bjornchristian.abrahamsen@sintef.no) (B.C. Abrahamsen).

<https://doi.org/10.1016/j.apor.2023.103774>

Received 13 June 2023; Received in revised form 11 October 2023; Accepted 12 October 2023

Available online 22 November 2023

0141-1187/© 2023 The Author(s). Published by Elsevier Ltd. This is an open access article under the CC BY license (<http://creativecommons.org/licenses/by/4.0/>).

anticipated.

Literature describing the local hydroelastic response of stiffened panels mounted on a vertical column and exposed to 3D wave hydrodynamic flow conditions is, to the knowledge of the authors, not previously studied. The local structural response due to wave slamming is affected by the local fluid mechanics of the impact, and the flexibility of the structure. A selection of relevant previous research on these topics are reviewed next.

The high local slamming pressures during wave impacts has been thoroughly researched for breakwaters and vertical sea walls. Bagnold (1939), Hattori et al. (1994) and Bredmose et al. (2023) studied wave impacts on a "rigid" vertical wall in a 2D wave tank. The largest impacts, in terms of pressure, were due to flat vertical wave front which enclosed a thin air pocket on the wall during the impact. The previous studies on vertical sea walls (Bagnold, 1939; Hattori et al., 1994; Bredmose et al., 2023) all show the importance of the air entrapment on slamming pressures, but they were all carried out in close to 2D conditions. The question remains of how important air entrapment/entrainment is for wave slamming loads in the 3D flow conditions relevant for ships and ocean structures? Intuitively, the air can more easily escape the area in between the breaking wave and the structure in the 3D case than in 2D case. In the presented model tests a high-speed camera system is used to film the impacts. The number of design critical wave impacts were air pockets and air entrainment are clearly visible on high-speed video is compared to the number of impacts where air is not visible.

Previous research on hydroelastic response during impact on calm water show that hydrodynamic slamming pressures are very sensitive to the details of the flow field, while the structural response (strains) measured are far less sensitive. Okada and Sumi (2000) compared measured slamming pressures with hydroelastic responses of a flexible wedge during drop tests. Both pressures and strains were measured during the impacts. The deadrise angle were varied from 4 to 0°. The hydrodynamics then changed from typical Wagner type of impact with travelling jets to that of an entrapped air cushion under the plate without jets. Hence, the pressure under the plate was very sensitive to the variation of the deadrise angle, while the maximum strains were far less sensitive to this variation.

Faltinsen (2006) did the same observation for the elastic response of a plate strip embedded in a nearly rigid rectangular plate during drop test impacts on waves with variable radius of curvature. He concluded that the maximum pressure was very sensitive to the local hydrodynamics of the impact while the maximum strains were not. Abrahamsen et al. (2020) studied the large plastic deformation of a plate during calm water impact for deadrise angles of 0 and 4°. He observed that the maximum indentation of the plate at a given impact speed were nearly equal in magnitude for the two deadrise angles. This means that the plates were not able to react to all details of the impact pressures and that the structure filters out a lot of the spatial and temporal content of the slamming pressures. This in turn motivated simplifications of the hydrodynamic models used in hydroelastic theory. Faltinsen (2006) showed that incompressible potential flow theory neglecting air entrapment did predict fairly accurate the maximum structural responses, even though the local details of the pressures were not captured in the theoretical model. The previous studies of impact pressures during drop tests show that the local pressures are sensitive to the geometry of the free surface prior and during impact. This argument is also relevant for wave impacts and can explain the large statistical variability of wave slamming pressures measured in model tests, see Lian (2018). On the other hand, hydroelastic drop test research shows that the local structural deflections are less sensitive to the local flow conditions than pressures. Is the same true also for wave impacts? That is, does extreme local structural responses show less variability than measured slamming pressures also when considering design critical wave slamming?

A major research question addressed in the present work is the design, manufacture, and instrumentation of relevant model-scale elastic steel panels at a scale of 1:40. The paper describes the scaling

laws, the design and the manufacture of relevant Froude-scaled elastic model panels which deflects, to scale, similarly to full scale stiffened steel panels. Modern 3D printing technology, combined with advanced material testing is employed in the design.

## 2. Froude scaling of stiffened steel panels

Fig. 1a) shows the structural details of one face of the full-scale steel column which is exposed to wave impact. The column is 16 m wide with a rectangular cross section and rounded corners. The part of the stiffened steel column which is modelled elastically is located within the red lines. Fig. 1b) shows this part, which is 5 m wide and 9 m tall, consisting of the outer plate, including vertical stiffeners and horizontal girders. Two different full scale steel panels are investigated, one strong and one weak. The cross-sectional dimensions of these panels are given in Table 1. The objective of the present paper is to design and instrument relevant Froude scaled elastic panels (image c), which is then used for the wave model tests at a scale of 1:40 (image d, e and f).

Scaling laws for the hydroelastic wave impact problem are derived using the Buckingham  $\pi$  theorem. This theorem requires the identification of a relevant set of physical parameters of the problem. The present problem is a wave with a nearly vertical wave front impacting on a column. The wave is dominated by the effect of gravity, which means that acceleration due to gravity  $g$  is a parameter of the problem. The wave impacts the column with a characteristic velocity  $V$ . The density of the water is  $\rho$ . Viscous and compressible effects of the water flow during the impact are neglected. The wave hits a vertical column with cross-sectional dimension  $L$ . Embedded in the front of the column is the stiffened steel plated structure indicated in Fig. 1d), and the geometry of the plate is described by a set of geometrical dimensions  $l_i$ . The stiffened steel plate is assumed to undergo linear elastic deformations with Young's modulus of steel  $E$ , and Poisson's ratio  $\nu$  and mass density  $\rho_s$ . Since, the objective of the present work is to design a stiffened plate which deforms as a full-scale stiffened steel plate, the deformation of the plate  $w$  is also a parameter of the problem. Hence, there are nine parameters of this problem which can be expressed as a combination of three fundamental units: length, mass and time. The Buckingham  $\pi$  theorem then states that there are six non-dimensional quantities. These quantities can be expressed as:

$$\frac{w}{L} = f\left(\frac{V}{\sqrt{gL}}, \frac{E}{\rho V^2}, \nu, \frac{\rho_s}{\rho}, \frac{l_i}{L}\right)$$

For the deformations to be similar in model and full scale, all nondimensional quantities need to be equal for the model and the prototype. Here,  $V/\sqrt{gL}$  is the Froude number which must be equal in model and full scale to provide similarity of the wave at the two scales. The nondimensional number  $E/\rho V^2$  represents the scaling of the Young's modulus. If all non-dimensional numbers are to be equal in model and full scale then all structural dimensions of the stiffened steel plate need to be geometrically scaled by a factor  $1:\lambda$ , where  $\lambda$  is the geometrical scaling factor. The ratio of the Young's modulus of the prototype,  $E$ , to the Young's modulus for the model material  $\bar{E}$  should be,  $E/\bar{E} = \hat{\tau}\lambda$ . Where  $\hat{\tau}$  is the density ratio of salt water to fresh water  $\hat{\tau} = \rho/\bar{\rho}$ .

For the present wave model tests the chosen scale is 1:40, but this part of the discussion is made general, considering a range of scales from 1:40 to 1:60. Fig. 2 shows Young's modulus and strength for different materials. This plot shows relevant materials for modelling of steel for this range of scaling ratios. For the full-scale steel panels in Table 1 the following parameters are assumed: Young's modulus 210 GPa, Poisson's ratio 0.3, yield strength 400 MPa and mass density 7850 kg/m<sup>3</sup>. The dashed black curve indicates the ranges of Young's modulus and strength values relevant for modelling steel in scaled models. The materials required to model typical steel structures for scale factors ( $\lambda$ ), ranging from 40 to 60 are materials with Young's modulus in the range 3.4–5.1 GPa. In addition, the elastic panels must be strong enough to

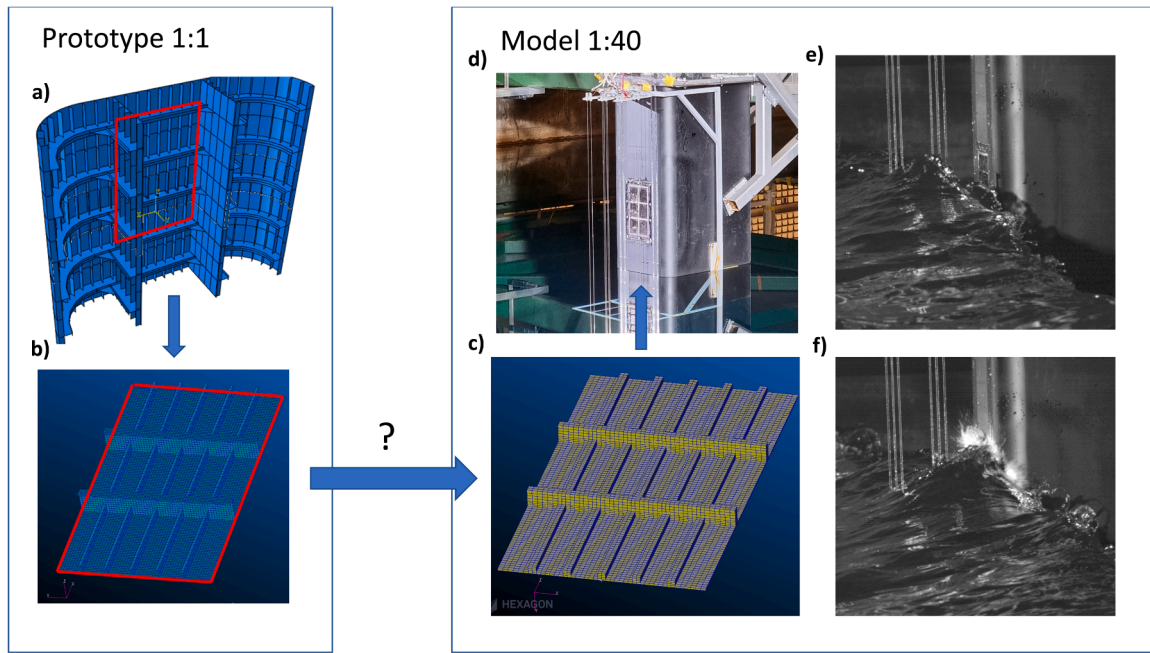
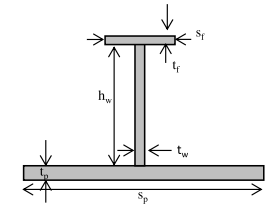


Fig. 1. (a) and (b) shows typical leg design of an offshore semi-submersible. Image (c) shows the approximate Froude scaled elastic panel representing the stiffened steel plate in (b). Image (d) shows the vertical column with the elastic model installed at a scale of 1:40 and image (e) and (f) shows a typical wave slamming event from the model tests.

**Table 1**  
Relevant full-scale dimensions of stiffened steel panels relevant for the strong and the weak 3D printed elastic panels.



Stiffened steel panel Dimensions	$t_p$ [mm]	$h_w$ [mm]	$s_f$ [mm]	$t_w$ [mm]	$t_f$ [mm]
<i>Strong plate</i>	18				
Stiffener		330	83	11	18
Girder		750	300	16	20
<i>Weak plate</i>	12				
Stiffener		240	83	7	12
Girder		430	200	11	13

survive many slamming events expected during the experiment. Hence, the strength of the model materials  $\bar{\sigma}_s$  should be at least as high as the scaled strength of the full-scale materials  $\sigma_s/(\hat{r}\lambda)$ . Therefore, the dashed black area is bounded for low material strength at  $\alpha = 1$ , where  $\alpha$  is the ratio of the model material strength to the full-scale material strength.

Fig. 2 shows that model materials which represents the elastic response of general steel structures cannot be made from any homogenous metal. The large class of materials categorized as polymers are relevant and homogenous thermosets applies. Polymer materials do however exhibit viscoelastic behaviour to various extents. This means that excessive structural damping may be of concern. Structural damping due to viscoelasticity may be controlled by choosing a polymer material with a sufficiently high glass transition temperature. An example of the latter is polycarbonate which was used to represent the

elastic behavior of concrete at a scale of 1:55 (Abrahamsen et al., 2023). For completeness concrete with a Young's modulus of 30 GPa and strength of 45 MPa (compression only) is also indicated in Fig. 2, and relevant range of the strength and modulus required according to the ideal scaling are indicated within the dashed blue lines.

The material needs to be evaluated in combination with the procedure of manufacture and its accuracy. Geometrical scaling of stiffened steel panels leads to thin models with some thicknesses far less than 1 mm. Secondly, the material should be homogenous, linear elastic and strong enough to withstand the many loading events expected during the wave experiment. Finally, the material and manufacturing method must support the instrumentation required to measure structural deformations.

In this work 3D printing is used to produce the elastic panels. 3D printing is attractive for manufacturing complex geometries. The panels were produced using a stereolithography (SLA) 3D printer which prints the model, layer by layer, using a photopolymerization process. The panels were printed with an iPro8000 from 3D Systems, using a layer height of 0.1 mm. The accuracy of the manufacturing process was investigated with test prints with plate thickness down to 0.6 mm. For this thickness, the plate warped inward and outward between stiffeners. Because of this problem all thicknesses of the final design were larger than 1 mm.

The elastic model panels were instrumented with strain gauges. The strain gauges, HBM Type 3/350 LY18, were installed. These strain gauges were large enough to be mounted accurately by hand. These strain gauges are 4.5 mm wide. Due to the size of the strain gauges, the thickness of stiffeners and girders were set to 4.7 mm. Furthermore, if the dimensions of the stiffeners and girders were scaled geometrically, the plate, stiffener and girders would be prone to undergo complex deformations when loaded. One concern was lateral torsional buckling of the stiffeners during impact, which cannot be monitored using a reasonable amount of strain gauges. These modes of motion would then be a major source of uncertainty in the model experiment which also motivated the simplifications of the stiffener and girder cross-sections.

For the present study, the 3D printing material "Accura ClearVue" from 3D Systems was selected. This material is a polycarbonate

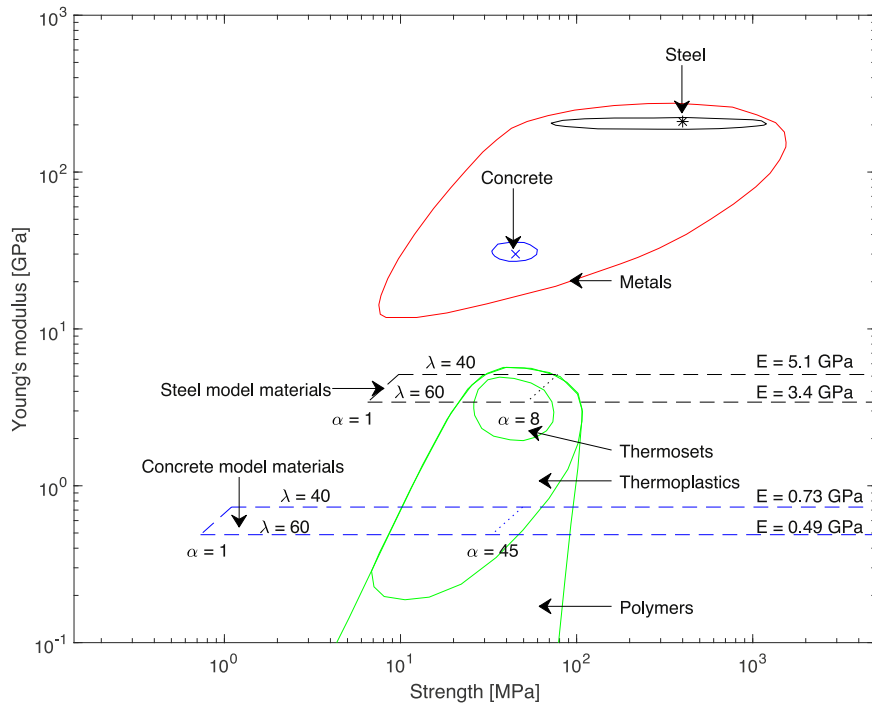


Fig. 2. Map identifying model materials which can represent the elastic response of steel (- -). The material data are obtained from [Materials Data Book \(2003\)](#).

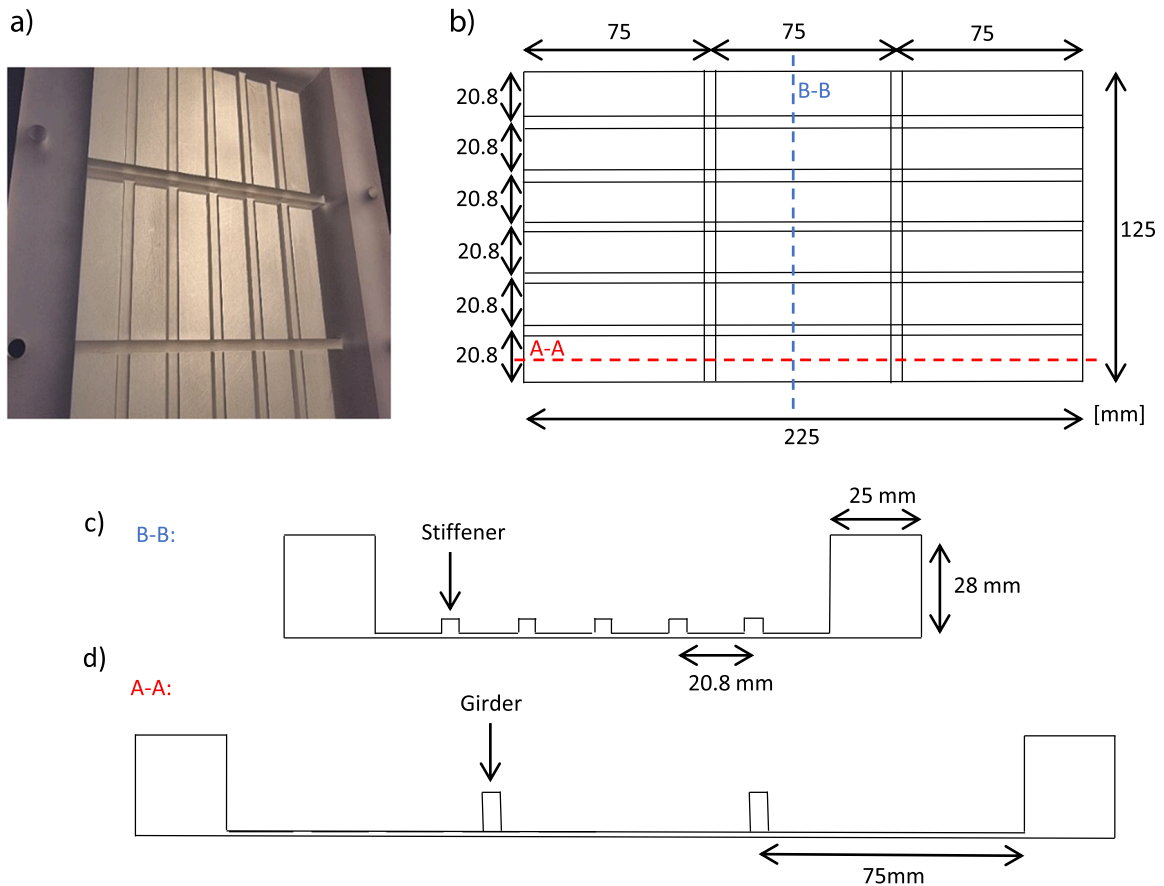


Fig. 3. Photograph showing the 3D printed Froude scaled panel from the inside (the strong panel). Illustration (a) shows the panel from the inside. Plot (b) shows the locations of the stiffeners and girders, (c) show cross section B-B and (d) shows the cross-section A-A.

imitation with a Young's modulus of 2.7 GPa and Poisson's ratio of 0.39 and a mass density of 1170 kg/m<sup>3</sup>. Fig. 3 shows a photograph of the final 3D printed panel. The drawing in b) shows the overall layout, and drawings c) and d) show cross section B-B and A-A. The elastic panel was printed surrounded by a strong frame with rectangular cross-section of 25 × 28 mm<sup>2</sup>. This frame was then bolted to the front face of the steel column during the wave impact tests (See Fig. 1).

Table 2 shows the dimensions of the strong and weak elastic panels resembling the strong and weak full scale steel panels specified in Table 1. The plate thickness and the widths of the stiffeners and girders were equal for both the weak and strong model panels, but the height of stiffeners and girders were different to obtain panels with different stiffness. The table contains dimensions as specified to the 3D printer, and measured dimensions of the actual printed model. These measurements were carried out using both a 3D scanner and a digital calliper. The dimensions are seen to deviate mainly in the direction normal to the plate. The plate thickness is higher than specified while the heights of the stiffeners and girder are lower than specified.

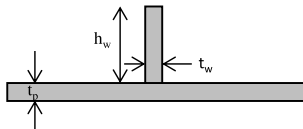
### 3. Material tests of the 3D printing material

Material tests were carried out to document the material properties of the 3D printing material. All polymers exhibit some degree of stress relaxation and creep. When these materials are subjected to a constant strain, the stress will reduce over time (relaxation). If the stress is constant, the strain will increase over time (creep). Also, the effective Young's modulus depends on the strain rate. Tensile tests including digital image correlation (DIC) measurements were carried out at two strain rates, 1 mm/min and 50 mm/min, to document the tensile modulus and the Poisson's ratio of the material. The measurements were taken using ISO 527 type 1A samples with a grip-to-grip distance of 115 mm. The resulting strain rates are much lower than the strain rates experienced during the wave impact tests, which reach a value of about 8 [1/s]. Therefore, torsional dynamic mechanical thermal analysis (DMTA) was carried out to determine the shear modulus at higher strain rates. Both the tensile data and the DMTA data were used together to fit Prony Series expansion (analogous to a set of N Maxwell elements in parallel) of the shear and bulk modulus:

$$g(t) = \sum_{m=1}^N G_m e^{(-\beta_m t)} \quad (1)$$

$$k(t) = \sum_{m=1}^N K_m e^{(-\gamma_m t)} \quad (2)$$

**Table 2**  
Dimensions of the elastic panels as *specified* (input to 3D printer) and as *measured* after printing.



Model geometry	Plate		Stiffener		Girder	
	Spec	Meas.	Spec	Meas.	Spec	Meas.
Model scale [mm]	t <sub>p</sub>	t <sub>p</sub>	h <sub>w</sub>	h <sub>w</sub>	t <sub>w</sub>	t <sub>w</sub>
<i>Strong plate</i>	1.0	1.10				
Stiffener			3.86	3.50	4.70	4.70
Girder			11.4	10.75	4.70	4.70
<i>Weak plate</i>	1.0	1.10				
Stiffener			1.97	1.82	4.70	4.70
Girder			7.10	5.90	4.70	4.70

Here,  $G_m$  and  $K_m$  are shear and bulk relaxation moduli and  $\beta_m$  and  $\gamma_m$  are decay constants. Two terms were found sufficient to match model and measurements. The identified parameters of the model were  $G_1=1.55 \cdot 10^8$ ,  $G_2=6.97 \cdot 10^8$ ,  $\beta_1=1.00$ ,  $\beta_2=1.00 \cdot 10^{-4}$ ,  $K_1=0.0$ ,  $K_2=3.639 \cdot 10^9$ ,  $\gamma_1=0.0$ , and  $\gamma_2=1.00 \cdot 10^{-5}$ . The corresponding Young's modulus is plotted in Fig. 4. For the material, the Young's modulus is according to Eqs. (1) and (2), 2.77 GPa, if loaded infinitely fast, and decays afterwards. The Poisson's ratio was also estimated from the tensile tests. Poisson's ratio was estimated to be 0.39 for the tensile tests at the highest strain rate, 50 mm/min.

The dimensions of the stiffened steel panel defined in Table 1 are selected to have approximately the same Froude scaled stiffness as the model panels defined in Table 2. This was carried out by comparing that static response of the panels when exposed to a uniform pressure on the wet side of the panel. This finite element (FE) analysis is explained in the following text. Fig. 5a) shows the solid element model of the strong elastic (test) panel while b) shows the corresponding shell element model of the strong stiffened (full-scale) steel panel. The FE analysis (FEA) were carried out in MSC Nastran (2019) using linear static analysis and standard finite elements which means QUAD4 shell elements for the full-scale panels and HEXA solid elements for the model panels. Linear elastic material models were applied. The Young's modulus is chosen to be 2.7 and 210 GPa for the model and full-scale panels and the Poisson ratio were set to 0.39 and 0.30 for the model and full scale panels. The FE models were fixed along the boundaries.

The full-scale steel panel were exposed to 1 MPa uniform pressure on the wet side of the plate while the model panel were exposed to a constant, Froude scaled pressure of 1 MPa/40/1.024. The wet side of the panel refers to the outer surface which is wetted by the impacting wave during the impact. Then the dimensions of the full-scale steel panel were adjusted in order to produce correct geometrically scaled deflections at the top of the girder and center stiffener. This meant that the target deflections of the full-scale steel panel were to be 40 times larger than for the model panel. This procedure was used for both the strong and the weak panels and the final dimensions are reported in Table 1. The static deflections of the full-scale panels were within 5 % of the geometrically scaled deflections of the model panels.

### 4. Instrumentation of the elastic model panels

Fig. 6a) shows the locations of the strain gauges mounted on the elastic section. Strain gauges were mounted on measurement points at the mid span of the center row of stiffeners. The strain gauges mounted on the girders were located in the middle between the adjacent

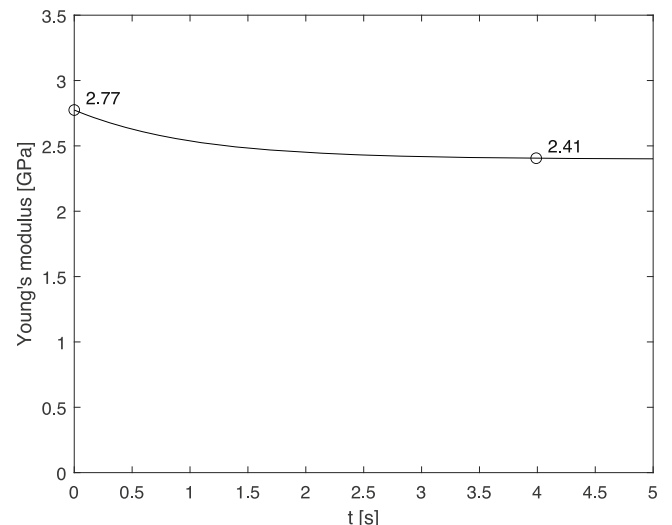


Fig. 4. Shows the Young's modulus as a function of time.

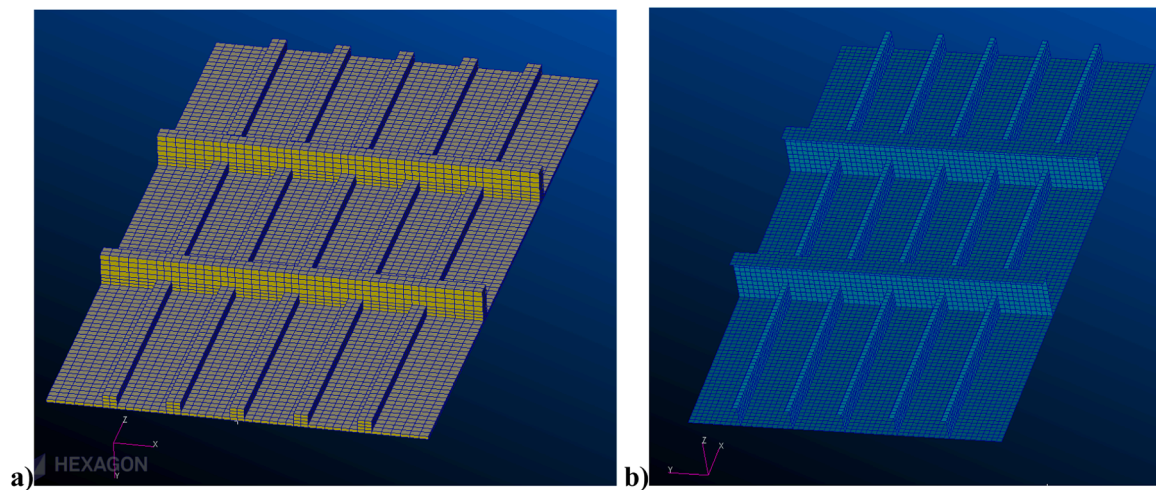


Fig. 5. Plot (a) shows the solid element model of the strong elastic panel at a scale of 1:40 and (b) shows the shell element model of the full scale strong stiffened steel panel.

stiffeners. The strain gauges were mounted in pairs at each measurement location, one on the top of the stiffener/girder and one on the wet side of the panel.

The elastic sections were tested by applying static loads at specific points on the stiffeners and girders. A cylindrical pin was mounted on a force transducer and the force transducer was mounted on a beam which was attached to a table with a hinge. Loads were added on a plate above the pin when located at the points F1 to F5, see Fig. 6b). Measurement of the applied force from the transducer connected to the pin was used to document the applied load. Fig. 6c) shows the measured girder strains at G1 due to load at that girder (at point F2) and strains at G2 due to load at that girder (at point F4). The plot shows that the strain in the girder G2 is higher than in G1. Due to symmetry of the model, these results should have been identical. The strain measurements are compared with static linear elastic finite element analysis. The mesh consists of the standard solid (HEXA) element formulation in MSC Nastran (2019). Two FE models, one of the strong and one of the weak elastic panel, were made according to the geometry of Table 2. The strain was compared 4 s after the load was applied. According to the viscoelastic material model in Fig. 4b), the Young's modulus is reduced to 2.41 GPa at this time. Poisson's ratio was 0.39 for the static FEA of the static force tests. Fig. 6c) shows the time series of strains at the girders of the strong panel when loaded at the girders (point F2 and F4). The strain from static FEA are indicated with black circles.

Table 3 shows the results of the static force tests for all strain gauges on the dry side of the two panels as described by the two first columns of the table. The dry side refers to the side of the panel containing the stiffeners and girders which is dry during the wave impact. In the third and 4th column are the measured load and the time it took to load the model. The 5th column is the measured strain which is compared with the static FEA in the 5th column. The last column shows the deviation between the FEA and measurements. For the centre stiffener for the strong panel FEA model is 12.5 % larger than measurements. For the lower stiffener of the weak panel the FEA is 10 % lower than measurements.

The deviations between measurement and FEA show the accuracy of the elastic panel and may be due to slight differences in the girder geometry and material of the real panels compared to the reported geometry (Table 2) and material parameters (Young's modulus and Poisson's ratio). Also, there is a chance that the deviations may be due to the strain gauge and panel assembly.

## 5. Hydroelastic wave impact experiment set up

Fig. 7a) shows a vertical cross section of the vertical column installed in the wave tank including dimensions. The elastic panel is indicated in grey and was mounted 168 mm above the mean free surface. Fig. 7b) show the horizontal cross-section of the column including dimensions. The vertical column was manufactured from steel plates and was fixed with a welded trusswork to the carriage. The vertical column was mounted 34.5 m from the wave maker as described in Fig. 7c).

The column was subjected to design-critical wave impacts, relevant for the north Atlantic. The irregular waves tested had a significant wave height,  $H_s$ , 13.3 m and spectral peak period,  $T_p$ , of 13.7 s following a Jonswap wave spectrum with a peak enhancement factor of 3.0.

The time series of the flap motion were generated using fast Fourier transform by dividing the wave spectrum in 3209 wave frequency components between 0.1 and 1.8 Hz (model scale frequencies). Each component was generated with a uniformly distributed random phase and a random amplitude following the Rayleigh distribution. Different realizations of this wave were generated which are denoted seed variations in the following text. The waves were calibrated and documented through separate wave measurements without the model in the wave tank. The model scale duration of each wave test was three hours divided by square root of the scaling factor 40. This corresponds to a duration of 3 h in full scale according to the Froude scaling law.

## 6. Characteristics of structural response due to design critical wave impacts

The vertical column including the elastic panels were installed in the towing tank and exposed to irregular waves. A total of 30 irregular waves were tested with the strong panel and 22 irregular waves with the weak panel. Each irregular wave test was assigned to a unique five-digit number, denoted a test number. The measured strain time series were analyzed to identify the wave impact events causing the largest strains for all the strain gauges located on top of the stiffeners, S1, S2 and S3 and girders G1 and G2 for all tests. The largest 8 events for the strong panel and the largest 6 events for the weak panel are shown in Table 4. The table contains the maximum strain value, the time of max strain relative to the start of the test in full scale seconds and the test number. Columns 2–5 of the tables show the maximum absolute strain values in%, while columns 6 to 9 shows the time of occurrence of the strain maximum and columns 10 to 13 shows the corresponding test numbers. Since the strain measured on the dry side were consistently higher than the strains on the wet side, only strains measured on the dry side is included. A

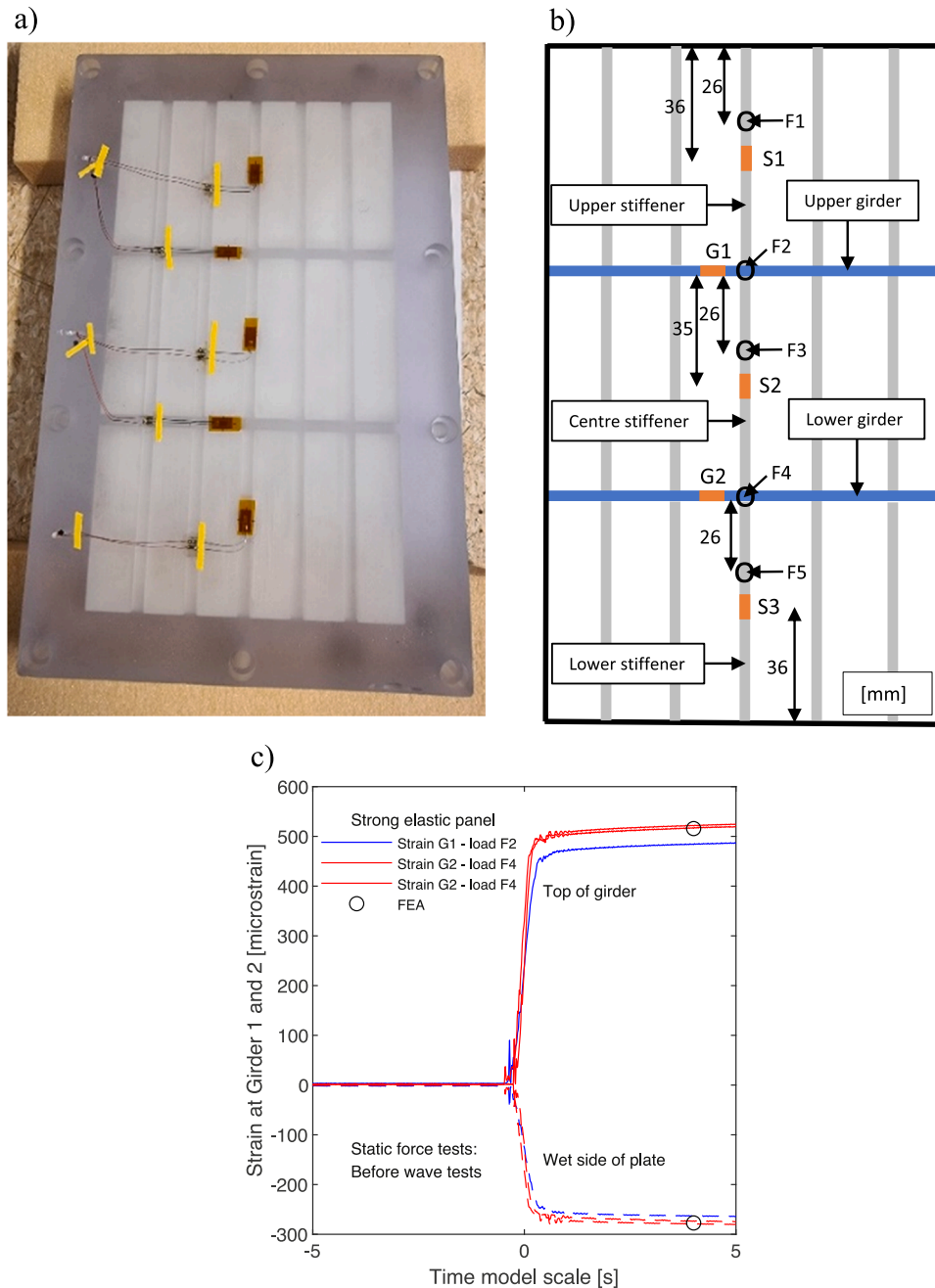


Fig. 6. (a) Photograph showing the strain gauges mounted on wet side of the elastic panel. Plot (b) show the naming convention on stiffeners and girders, strain measurement points S1, G1, S2, G2 and S3, and location of applied forces during static force testing F1-F5. Plot (c) shows time series of measured girder strains due to point load at girders for the strong elastic section.

longer list of events are provided in Tables A1 and A2 of the Appendix.

Table 4 shows that the maximum strains are generally larger for the weak than for the strong elastic panel. However, the largest maximum strain, 0.97 %, was recorded for the strong elastic plate at the centre stiffener (stiffener 2).

Three high speed cameras operating at 1 kHz were mounted to study the fluid mechanics of the severe wave slamming impacts. The cameras were triggered by the strain measurements. The system automatically transferred the high-speed images from the rapid memory located on the cameras to a hard drive storage on a dedicated computer. The vertical column was painted black to maximize contrast between the air entrapped and the background. Fig. 8 shows high speed video recorded for the largest strain event for the strong model panel, which occurred on test 30,111, 5970 s. after the start of the 3 h irregular wave test. The

vertical column is seen from the side, front and at a 45-degree angle in the images A, B and C.

The high-speed videos were used to study physics of the wave impact and identify entrapped and entrained air during the impact. Fig. 9 shows images of the three slamming events generating the largest strains on the center stiffener (Stiff. 2) for the strong elastic panel. High speed videos of the impact in the format shown in Fig. 8 are linked in (a) and (b). The second largest impact shows little, or no air entrapped during the impact. While visible air is entrapped in the largest impact and in the third largest impact. A rough measure of how frequently visible air is entrapped during large wave slamming events was obtained by studying the high-speed videos. For the strong elastic section, the 8 largest maximum events (in terms of strain at the centre stiffener) out of a total of 30 realizations, were investigated. For the weak elastic section, the 6

**Table 3**  
Static force tests for documentation of elastic panel accuracy. Comparison of measured and calculated FEA strains due to static point load.

Strain point	Load point	F [N]	$\Delta t$ load [s]	Meas. [microstrain]	FEA [microstrain]	FEA deviation %
<b>PANEL STRONG</b>						
S1	F1	9.75	0.60	637	655	2.9%
S2	F3	9.71	0.60	684	769	12.5%
S3	F5	9.75	0.52	639	684	7.1%
G1	F2	19.21	0.70	480	516	7.4%
G2	F4	19.45	0.47	515	516	0.1%
<b>PANEL WEAK</b>						
S1	F1	4.85	1.22	545	556	2.0%
S2	F3	4.85	1.63	601	644	7.2%
S3	F5	4.87	0.93	641	577	-10.1%
G1	F2	9.79	1.43	640	683	6.8%
G2	F4	9.74	1.37	648	683	5.5%

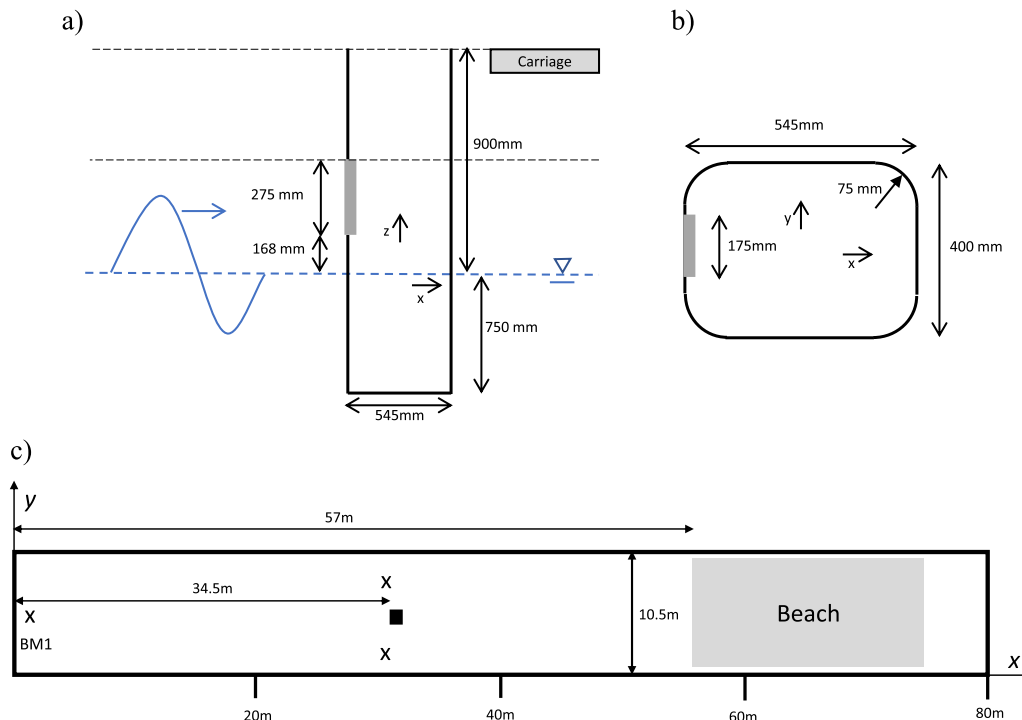


**Fig. 7.** Sketch (a) shows the main dimensions of the vertical column and the location of the elastic panel (indicated in grey). Sketch (b) shows the cross-sectional dimensions of the column and (c) shows the location of the column in the wave tank. All model scale dimensions.

largest events out of a total of 22 realisations were investigated. The high-speed videos show that, for the strong elastic section out of the 8 largest impacts show no visible air entrapment during the slam, while for the weak elastic panel 2 out of 6 largest impact events showed no visible air entrapment.

Fig. 10a)–c) show the strain time series recorded during the three largest slams for the centre stiffener of the strong elastic panel shown in Fig. 9. Fig. 10d), e) and f) show the corresponding time series for the three largest events for the centre stiffener of the weak panel. The black lines indicate strains measured on top of the stiffeners and girders on the dry side of the panel, while red lines indicate strains measured on the wet side of the panel. Each plot a)–f) show 5 different plots. From top to bottom these show time series of the upper stiffener (S1), upper girder (G1), centre stiffener (S2), lower girder (G2) and lower stiffener (S3), respectively.

The time series shows that for all three impacts, for both the elastic panels, the two girders and the center stiffeners reach positive amplitudes at the same time. This suggests that the deformations at these

locations can be well described by a global mode of motion. Studying the time series of the 4th, 5th and 6th largest events for the center stiffener shows the same trend for both panels.

The responses of the panels for the largest strain events are compared next. The strain time series is made nondimensional by dividing the strain by its maximum value listed in Tables A1 and A2. Fig. 11 shows the normalized time series of the response for the largest 15 maxima recorded on the upper, (a), center, (b), and lower stiffener, (c), of the strong elastic panel. Plot (d), (e) and (f) show similar plot for the weak elastic panel. Fig. 12 shows the normalized strain time series measured on the girders of the strong elastic panel, (a), (b) and weak elastic panel (c) and (d), for the 15 largest maximum events measured on the respective girders.

In most cases the strain time series of the stiffeners and girders obtain its maximum value during the first half period of vibration. Furthermore, the vibration of the structure is characterized by a limited frequency content, and the vibrations generally show strong decay after the time of maximum strain.



**Table 4**

Identification of the ~25 % largest slamming events with respect to measured strains inside the panels and the corresponding test number and time of maximum. Table a) strong elastic panel, b) weak elastic panel. Full scale data.

**a)**

Rank	Maximum strain inside panel					Time of max  strain					Test number				
	[%]					[s]									
	S1	G1	S2	G2	S3	S1	G1	S2	G2	S3	S1	G1	S2	G2	S3
1	0.592	0.740	0.968	0.711	0.616	9319	5970	5970	5970	5970	30120	30111	30111	30111	30111
2	0.469	0.379	0.622	0.488	0.291	5970	11271	5625	11271	11271	30111	30111	30080	30111	30111
3	0.443	0.354	0.558	0.365	0.281	6685	9319	11271	5625	5625	30100	30120	30111	30080	30080
4	0.386	0.295	0.486	0.297	0.271	6872	2303	9319	9319	8505	30170	30100	30120	30120	30220
5	0.306	0.268	0.452	0.275	0.258	4211	5625	6393	6393	1313	30130	30080	30030	30030	30250
6	0.287	0.245	0.424	0.233	0.250	10700	10700	2303	8505	6135	30290	30290	30100	30220	30140
7	0.271	0.243	0.420	0.233	0.242	11241	6685	3690	3690	9319	30230	30100	30160	30160	30120
8	0.271	0.231	0.308	0.227	0.231	11601	6393	2460	2303	3680	30070	30030	30203	30100	30180

**b)**

Rank	Maximum strain inside panel					Time of max  strain					Test number				
	[%]					[s]									
	S1	G1	S2	G2	S3	S1	G1	S2	G2	S3	S1	G1	S2	G2	S3
1	0.640	0.820	0.553	0.663	0.680	2629	7730	7730	8200	8200	40060	40010	40010	40080	40080
2	0.638	0.579	0.552	0.653	0.614	7730	2306	6396	1231	10142	40010	40100	40030	40050	40190
3	0.580	0.555	0.545	0.551	0.505	4214	11604	8200	6396	1231	40130	40070	40080	40030	40050
4	0.565	0.551	0.522	0.521	0.404	2183	1312	1312	7730	7730	40120	40010	40010	40010	40010
5	0.557	0.547	0.499	0.479	0.381	11604	2629	6138	1312	4717	40070	40060	40000	40010	40210
6	0.541	0.547	0.498	0.455	0.358	4832	4214	1454	2306	7042	40210	40130	40000	40100	40000

Figs. 13 and 14 show color plots of the power spectra of the normalized strain time series shown in Figs. 11 and 12. The power spectrum was plotted for frequencies larger than 5 Hz to focus on the elastic structural vibrations. For the strong elastic panel, Fig. 13, the vibration of the center stiffener is dominated by two frequencies: one low frequency of about 20–23 Hz and the other an intermediate frequency of about 31–33 Hz. For the strong elastic panel the upper stiffener shows less vibration at the low frequency but vibrates more at the intermediate frequency and also at a high frequency of about 36 to 38 Hz. The lower stiffener behaves similarly to the upper stiffener. Both girders of the strong elastic panel oscillate with the low frequency ranging from 20 to 23 Hz while the upper girder also vibrates with a intermediate frequency ranging from 31 to 33 Hz.

For the weak elastic panel the girders vibrate with frequencies in the range of 12 to 14 Hz. These frequencies also dominate the response of the centre stiffener. The upper and lower stiffener show vibrations also at a higher frequency range from 17 to 22 Hz, in addition to the low frequencies of the girder vibration. The structure responds as one structural system, with few dominant modes, rather than a set of independent plates, stiffeners and girders.

In the following text the hydrodynamic added mass is estimated. It is assumed that the responses are due to free vibration in water and that there is no air entrapped between the free surface and the structure. The structural deformation is expressed using one dry eigenmode obtained from FE modal analysis. The dry natural modes associated with the three lowest dry natural frequencies for the strong elastic panel are shown in Fig. 15a).

The mode associated with the lowest dry natural frequency is used to

express the free vibrations of the wet panel since the girder strain and centre stiffener strain are in phase for this mode. This is then consistent with the observations from the measured time series. The wet natural frequency is given by:  $f_w = \sqrt{K/(M + A)}/2\pi$ . Here  $K$ ,  $M$  and  $A$  are the modal stiffness mass and added mass, and  $f_w$  is the wet natural frequency. The dry natural frequency  $f_d$  can be obtained by setting  $A = 0$ . An estimate of the hydrodynamic modal added mass to the structural modal mass can then be expressed as a function of the dry to the wet natural frequency:

$$\frac{A}{M} = \left(\frac{f_d}{f_w}\right)^2 - 1$$

The FE eigenvalue analysis shows that the full-scale natural frequency is 110.2 Hz and 68.7 Hz for the strong and weak elastic panels, respectively. From the wave impact tests, the lowest full-scale wet natural frequency of the strong and weak elastic panel is about 21.5 and 13.0 Hz. This is based on the power spectra in Figs. 13 and 14. The ratio of added mass to structural mass is then calculated to be 25.3 and 26.9 for the strong and weak elastic panels, respectively. This means that the added mass of the elastic panel is much larger than the structural mass. This supports the assumption that the structural mass does not need to be very accurately modelled since the structural mass is a small part of the effective mass.

The power spectra presented in Figs. 13 and 14 provide limited information on what temporal resolution of the measurement which is required to capture the maximum responses. The experiments were carried out with a sampling frequency of 19.2 kHz (model scale) which was filtered at 6 kHz (model scale) before storing the data.

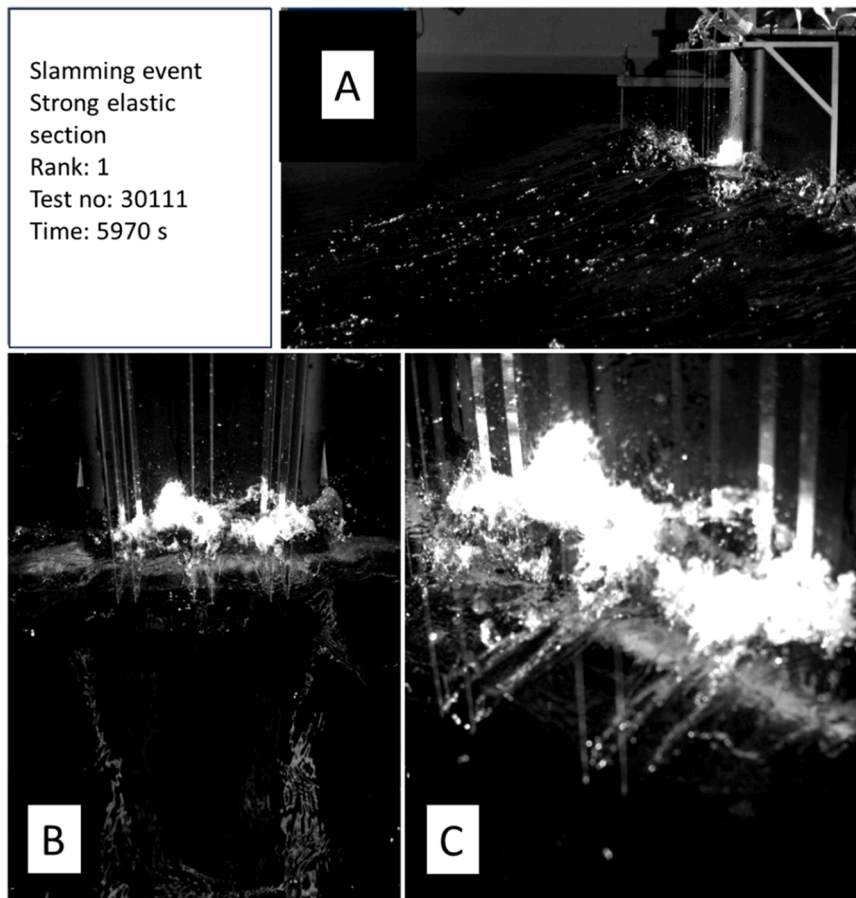


**Fig. 8.** Format of the high-speed video recordings linked to Fig. 9. The videos show high speed video from three angles to study the local fluid mechanics of the slamming impact.

This high sampling frequency is equal to the sampling frequency often used for local slamming pressure measurements. Slamming pressure measurement require very high sampling frequency since the slamming pressures have very short duration. The question is if the measured strain time series could have been acquired on a lower sampling rate? To investigate this question the time series were filtered digitally on 80 Hz (full scale) to see the effect on the measured strain peaks. Fig. 15 shows the *measured response* time series at the stiffeners, b), and girders, c), during the impact causing the 2nd largest maximum strain on the centre stiffener (test: 30,080 t:5625 s). The blue curves are the original measurements while the red curves are filtered on 80 Hz (full scale) which corresponds to 506 Hz in model scale. The peak structural response is not modified significantly by this filtering. This filtering exercise shows that practically the same strain time series could have been obtained with a much lower filter frequency. As an example, if the experiment were to be carried out again, a filtering frequency of 1 kHz would be sufficient since it is twice the frequency sufficient to describe the critical strain events. This is 6 times lower than the filtering frequency used in the model test. This means that the sampling frequency could have been lowered by the same factor, which simplifies this type of model tests significantly.

The measured strains during wave slamming plotted in Fig. 10 show large decay. Since viscoelastic materials contain damping, it was investigated if this source of structural damping could explain this decay. Transient finite element analysis of the strong elastic panel was carried out using *LS-Dyna Finite element software* (2023). A uniform mass of 50 kg/m<sup>2</sup> was added to model the hydrodynamic added mass (this corresponds to 2000 kg/m<sup>2</sup> at full scale). The viscoelastic material defined in Eq. (1) and (2) were used. The panel was exposed to a

spatially uniform pressure of short duration and the decay of the strain time series were investigated to study the viscoelastic damping. The time series showed less than 1 % damping. This means that viscoelasticity cannot explain the large decay of the structural vibration during the wave impacts.

## 7. Extreme value statistics of local structural response

The statistical properties of the structural responses are important from a design perspective. Proper extreme value statistics were carried out by identifying the largest measurements on the stiffeners and girders for each 3-hour realization of the irregular wave. Since the measured strains were consistently higher on the dry side of the panel than on the wet side, only the five measurement locations on top of the stiffeners and girders were considered. The tables identifying extreme strains are given in Tables A3 and A4 (see Appendix). The same extreme values are plotted in a Gumbel paper in Fig. 16.  $F$  on the y-axis is the probability that the extreme strain  $X$  is lower or equal to the value indicated on the x-axis. Plot a) and b) show the extreme strain of the stiffeners and girders for the strong panel, while plot c) and d) show the corresponding extreme strains of the weak panel. The plots and tables for the strong panel shows that there is one extreme strain event which is much larger than the others, which occurred at 5970 s of test 30,111. This event caused the largest strain on all members except the upper stiffener.

The statistical variability of the extreme values affects the confidence intervals of estimated  $q$ -probability responses. The coefficient of variation, defined as the standard deviation to the mean of the sample is a measure of the statistical variability and was calculated for both panels. Fig. 17 shows the coefficient of variation (COV) calculated for the

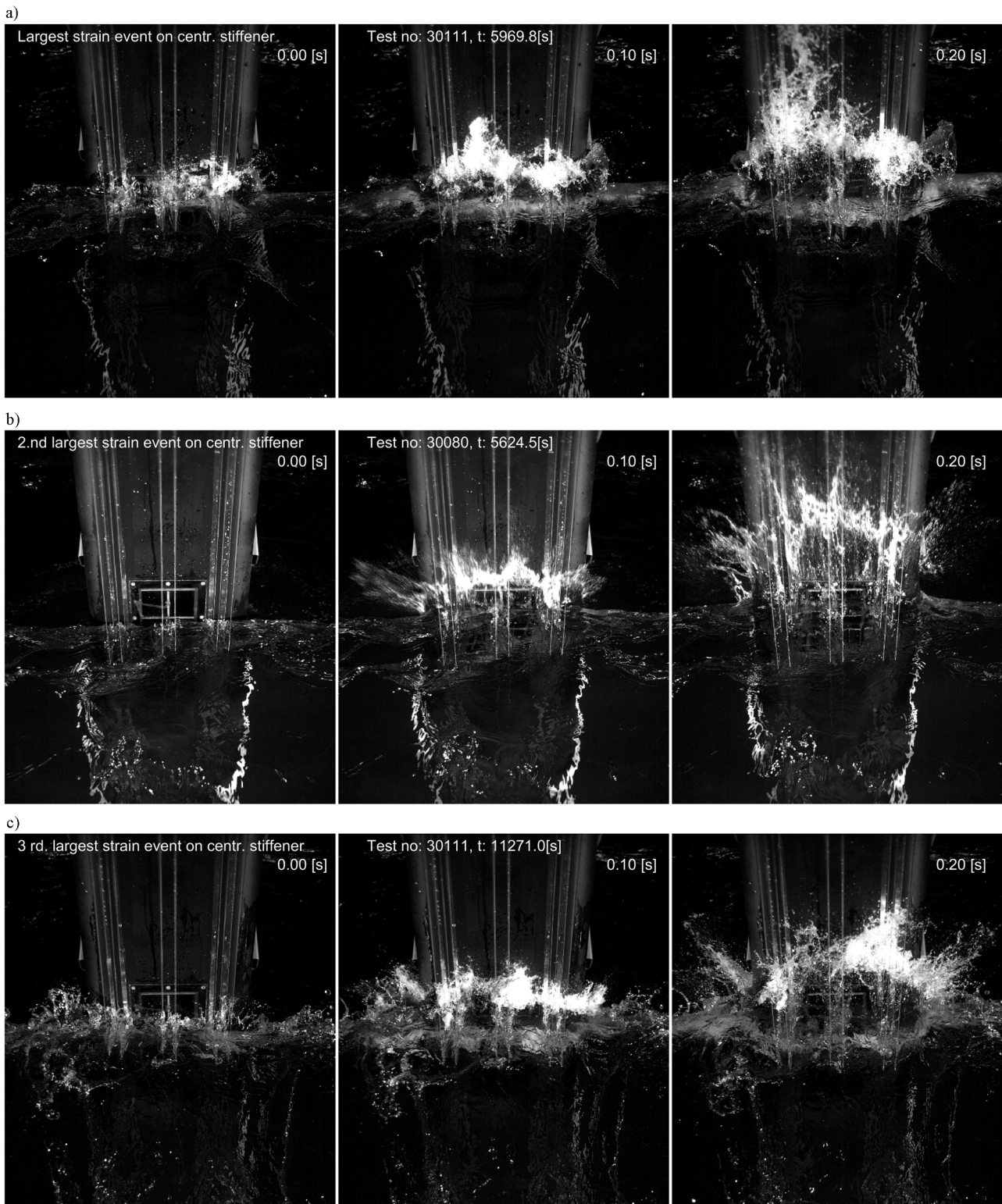


Fig. 9. Photographs of the slamming events causing the three largest maximum strains on the center stiffener of the strong elastic panel. *Multimedia attached to image a) and b).*

extreme strains of the stiffeners and girders for the strong panel (blue bars) and weak panel (red bars). The coefficient of variation is the sample standard deviation divided by the mean of the extreme values. The COV is in the range of 0.72 to 1.03 for the strong elastic section and between 0.36 and 0.64 for the weak elastic section. The value of COV for the girders are of similar magnitude as the COV for the stiffeners for both

panels.

The COVs of the strains can be compared with typical values of COV of other parameters. Lian (2018) studied the undisturbed long crested extreme wave crest heights and found COVs in the range from 0.06 to 0.1. He also studied the extreme wave slamming pressures on a  $3 \times 3 \text{ m}^2$  area, located 12 to 15 m above the mean water level, on a circular

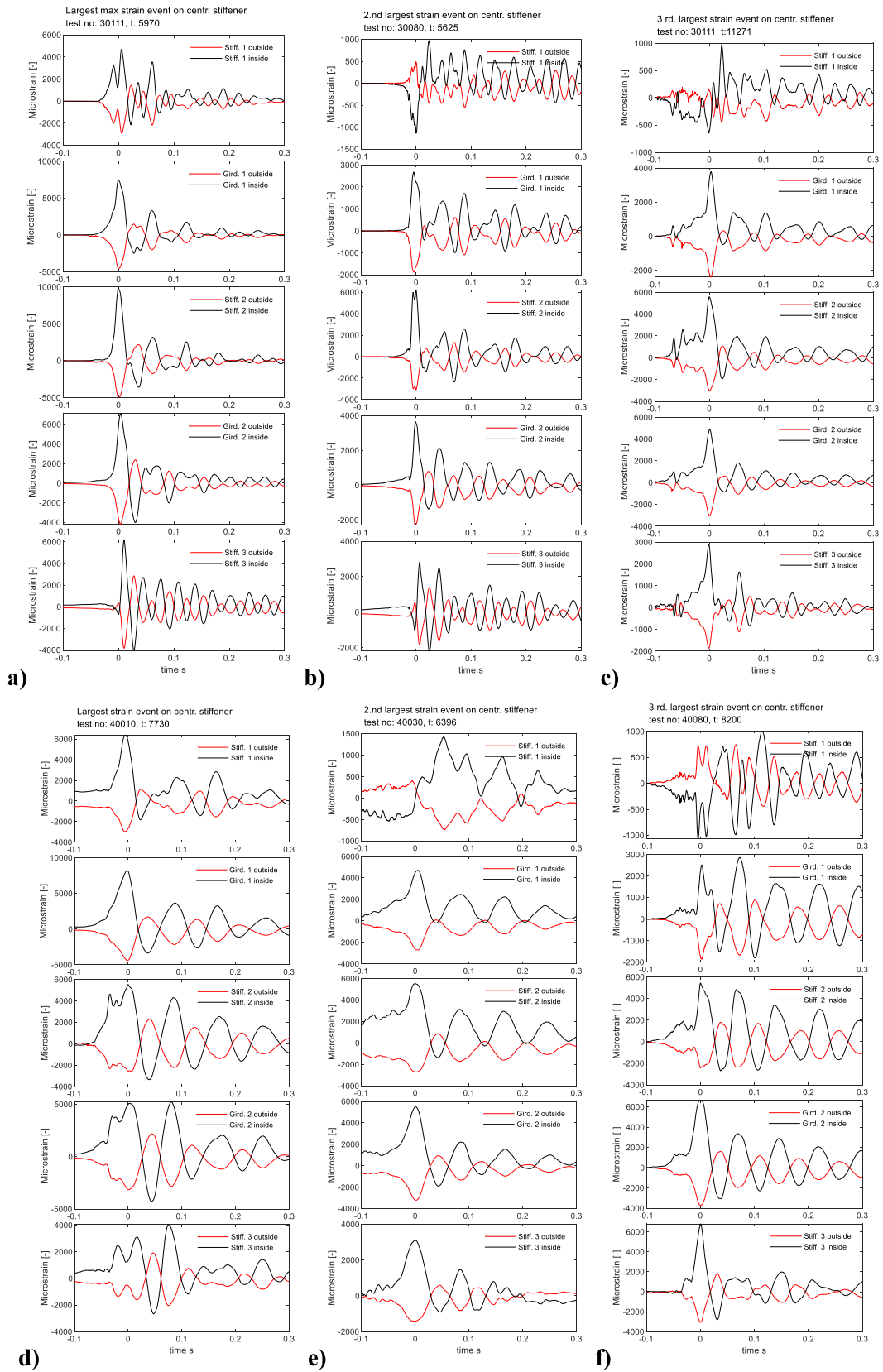
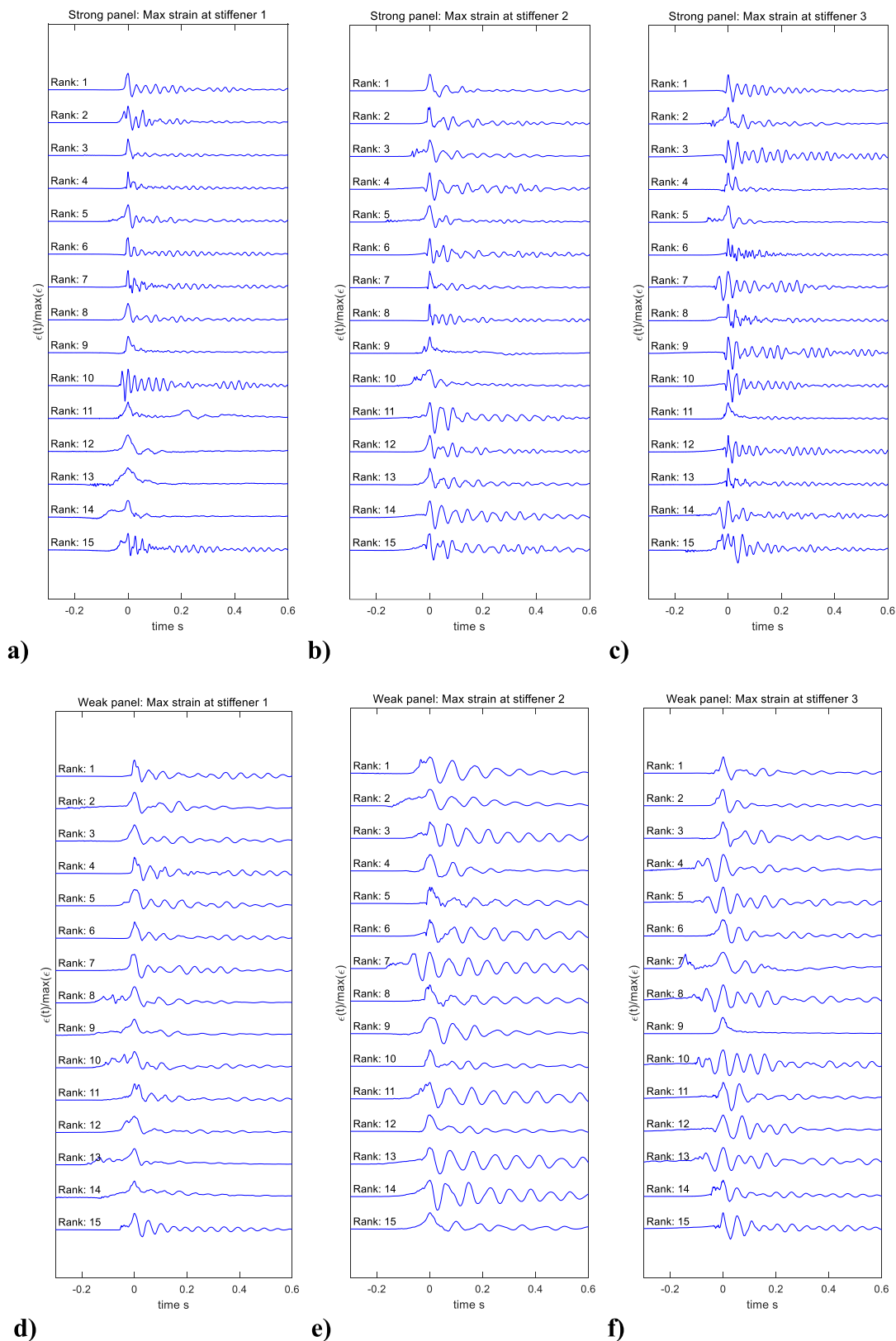
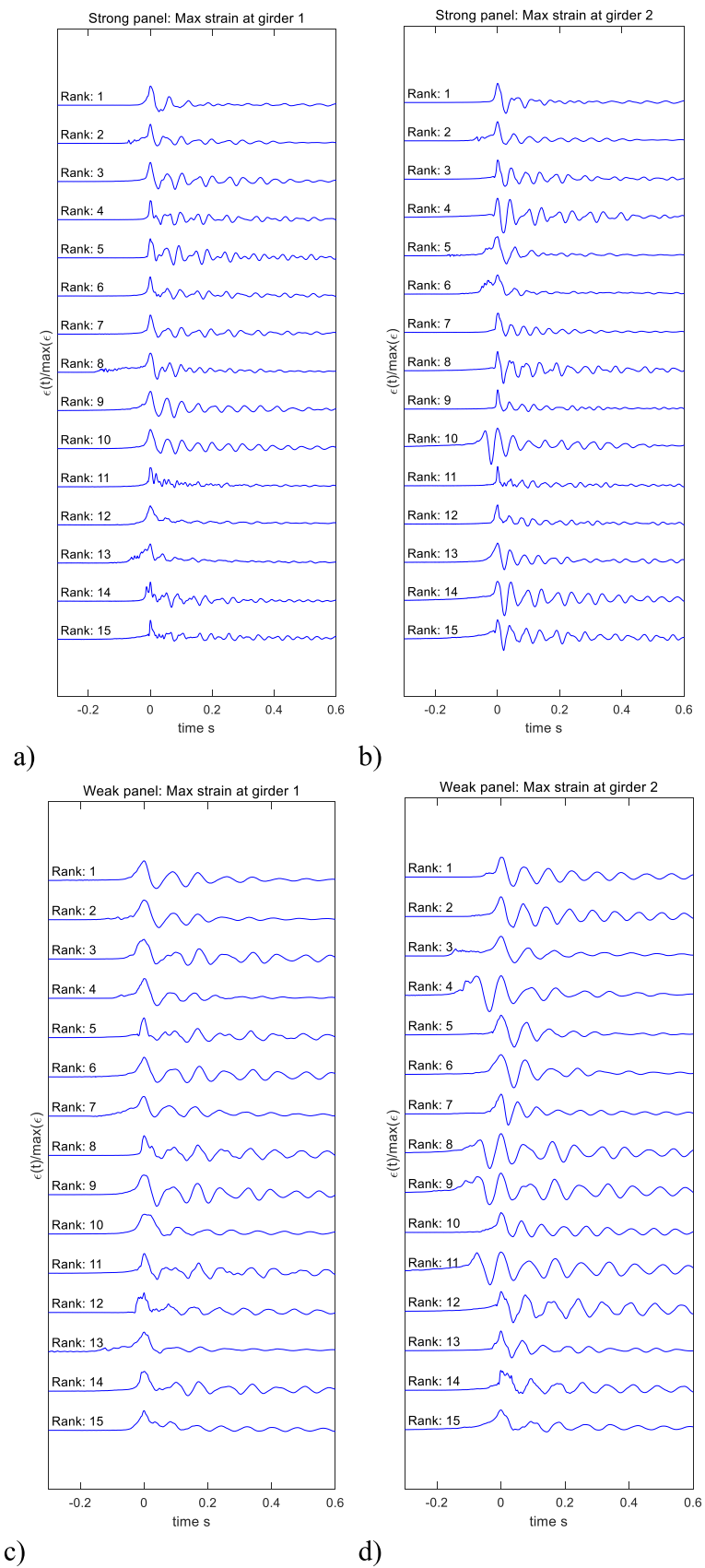


Fig. 10. Slaming event causing the three largest max strain on the center stiffener for the strong panel, (a), (b) and (c) and weak panel, (d), (e) and (f). Vertical order of each plot: strains on upper stiffener, upper girder, center stiffener, lower girder, and lower stiffener.



**Fig. 11.** Strain time series measured at the inside of the stiffeners, divided by its maximum value listed in Tables A1 and A2. Stiffeners of strong elastic panel, a), b), c) and weak elastic panel, d), e) and f).



**Fig. 12.** Strain time series measured at the inside of the girders, divided by its maximum value listed in [Tables A1](#) and [A2](#) (see Appendix). Girders of the strong elastic panel, a), b) and weak elastic panel, c) and d).

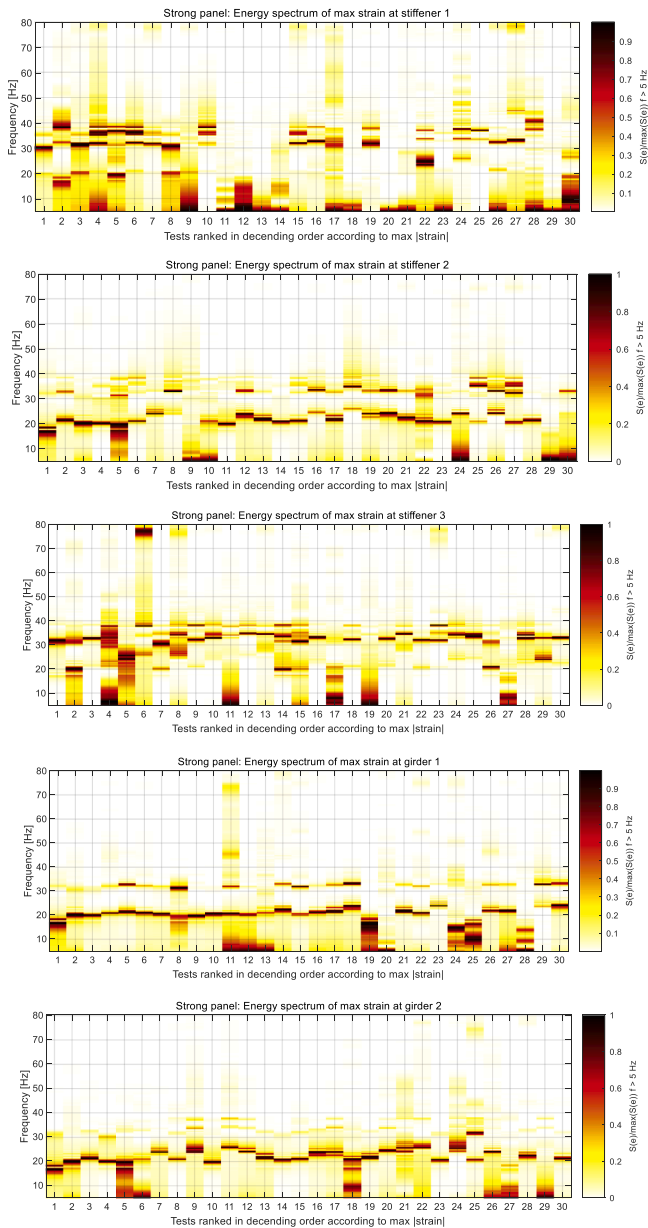


**Fig. 13.** Nondimensional power spectra of the strain time series recorded on top of the stiffeners of the strong elastic section for the 30 largest maximum strain events,  $\max|\epsilon|$ .

column with diameter 31 m, and found COVs in the range from 0.5 to 1.0. It should be noted that a threshold of 300 kPa were used, and extreme pressures below this threshold were eliminated from the sample. Comparison of the COVs of Lian with the extreme strains measured here, it is noticeable that the extreme strains of the strong elastic panel show COVs in the same range as the extreme pressures reported by Lian, and that the extreme strains measured on the weak panel is lower than for the strong panel. It should be noted that the COV depends on the threshold used in Lian's work. The Gumbel distribution were fitted to the measured data. The Gumbel distribution is defined as:

$$F(X \leq x) = \exp\left\{-\exp\left[-\left(\frac{x-\mu}{\sigma}\right)\right]\right\} \quad (3)$$

The parameters  $\mu$  and  $\sigma$  were fitted using the method of moments:  $\mu = m_M - 0.57722\sigma$ , and  $\sigma = \sigma_M/1.28255$ . Here  $m_M$  and  $\sigma_M$  are the sample mean and standard deviation. The fitted Gumbel distributions are plotted on top of the samples in Fig. 16.

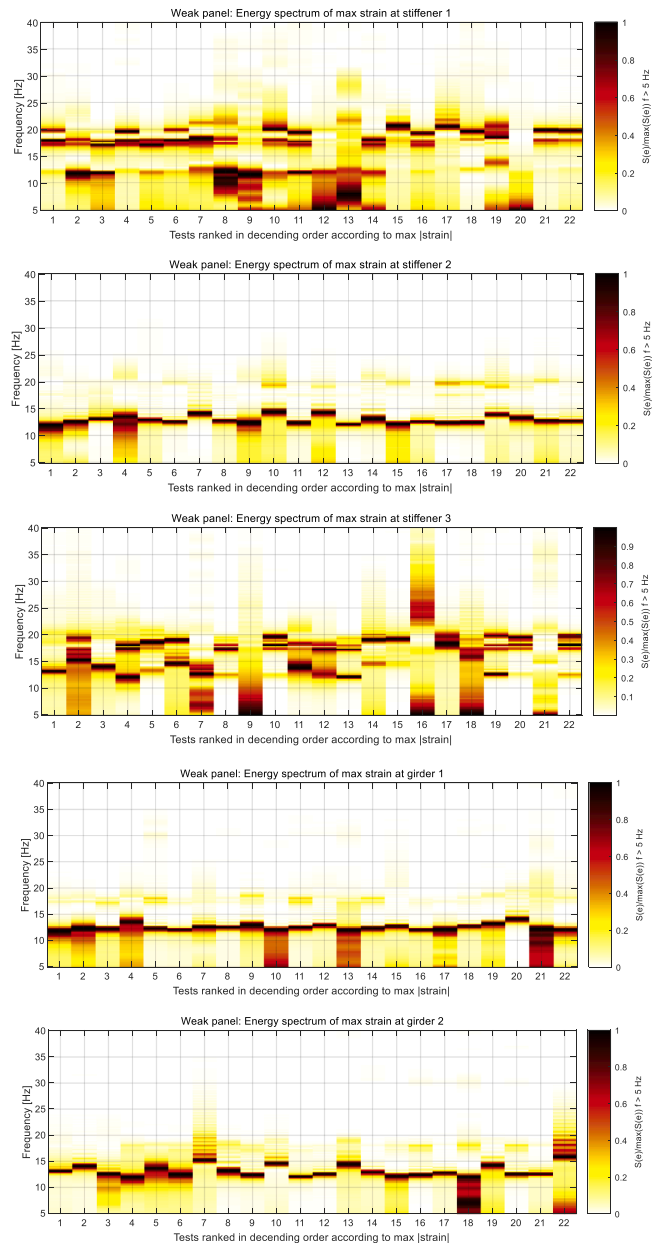


**Fig. 14.** Nondimensional power spectra of the strain time series recorded on top of the stiffeners of the weak elastic section for the 22 largest maximum strain events,  $\max|\epsilon|$ .

The accuracy of the Gumbel distribution was assessed by plotting quantile-quantile plots (Q-Q plots). Fig. 18 shows the Q-Q plot for the stiffener a) and girder b) for the strong panel and stiffener c) and girder d) of the weak panel. Q-Q plots does not quantify how well the Gumbel distribution represents the data and require visual interpretation. The strains for the strong panel deviate somewhat to the unconservative side while the strains on the weak panels show a reasonable fit to the Gumbel distribution.

### 8. Mechanical testing after wave tests

The static force tests were repeated after the wave impact tests for the strong panel. Table 5 shows the measured strain before and after the test in column 3 and 4. The deviation in less than 4 % for all except the lower girder (G2). This may be due to a crack developing during the test. High speed video images taken during the wave impact tests shows the

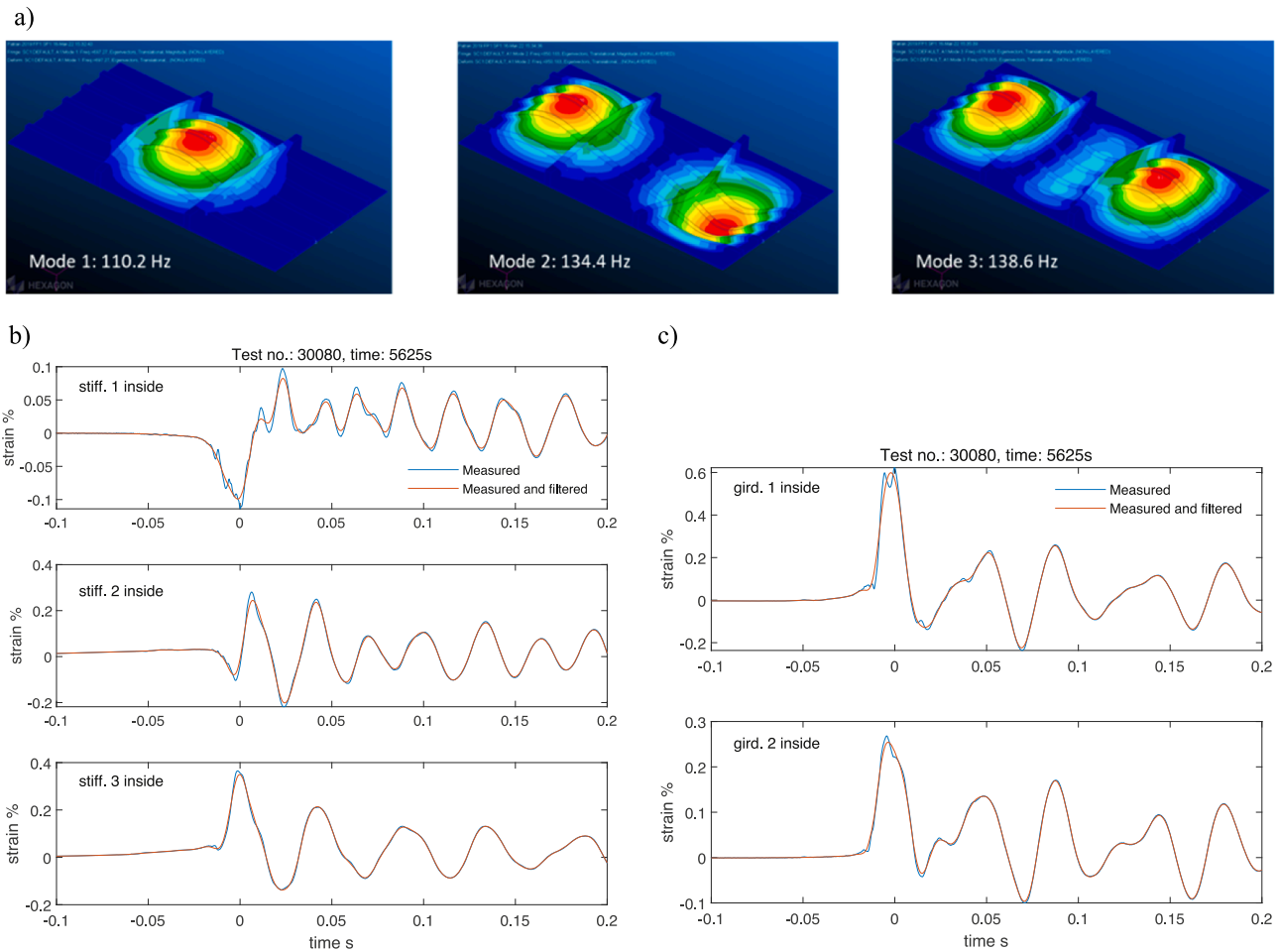


**Fig. 15.** a): The eigenmodes corresponding to the three lowest natural frequencies of the strong elastic panel. b) and c) show the effect of filtering the time series at 80 Hz (full scale) on the measured time series. Blue curves are unfiltered red curves are filtered time series.

crack development. The photograph in Fig. 19a) shows this crack near the left end of the lower girder. The crack was seen to grow during the tests. The high-speed videos were used to identify the time when the crack was initiated, and all tests containing visible cracks were discarded and are not included in the analyses presented herein. The weak elastic panel were damaged during a critical slam experienced during the 23rd three-hour wave test. Fig. 19b) shows one frame of the elastic panel during the critical wave impact. The image shows the lower girder G2. A part of the girder towards the rectangular frame broke off and shot inwards. The loose part left an opening in the column where water flew into the column. The high-speed videos of the wave impact tests carried out prior to this impact were investigated and no cracks or damage were identified prior to the critical event. Based on the high-speed video study a total of 30 successful realizations of the 3 h irregular wave were identified for the strong elastic panel and 22 realizations for the weak elastic panel.

**9. Summary and discussion**

A fixed vertical column representative of one leg of a large semi-submersible was tested at a scale of 1:40. The wave impact tests were performed in irregular wave conditions relevant for the North Atlantic, with significant wave height of 13.3 m and peak spectral period of 13.7 s. The wave impact tests were successfully carried out for 30 three-hour wave tests for the strong elastic panel. A total of 22 three-hour wave tests were carried out for the weak elastic panel.

The elastic panels were 3D printed, and the printing material was tested to determine relevant values for the tensile Young’s modulus and

Poisson’s ratio. The geometry of the printed panels were documented using a combination of 3D scanning and manual measurements with a calliper. The panels were instrumented with strain gauges and the final elastic panels were mechanically tested prior to the wave tests by static force tests. The accuracy of the panel response was documented through comparisons with FEA. The largest discrepancies were observed for the centre stiffener of the strong panel and the lower stiffener of the weak panel, for which FEA overpredicted the strain by 12.5 % and under-predicted the strain by 10.1 %, respectively. For the girders the FEA overestimated the strain at the upper girder by 7.4% for the strong panel and 6.8 % for the weak panel. The static force tests were repeated after the wave impact tests for the strong elastic panel. A comparison of the static tests before and after the wave impact tests showed that the static strains differed less than 4 % except for the lower girder which showed a deviation of 11.1 %. The large strain discrepancy for the lower girder was most probably due to the crack that developed near the lower girder during the tests.

The final produced elastic panels deviate from the ideal scaling laws laid out by the Buckingham  $\pi$  theorem in several ways:

- (1) The geometrical scaling of the panel should have been applied, however the accuracy of the 3D printer limited the thickness of the printed plates not to be less than 1 mm. Furthermore, complex structural response like tripping of stiffeners were not wanted since it is hard to detect using a reasonable number of strain gauges.
- (2) The Young’s modulus should have been higher  $\sim$ 5.3 GPa and the Poisson’s ratio should have been 0.3 while the material used for



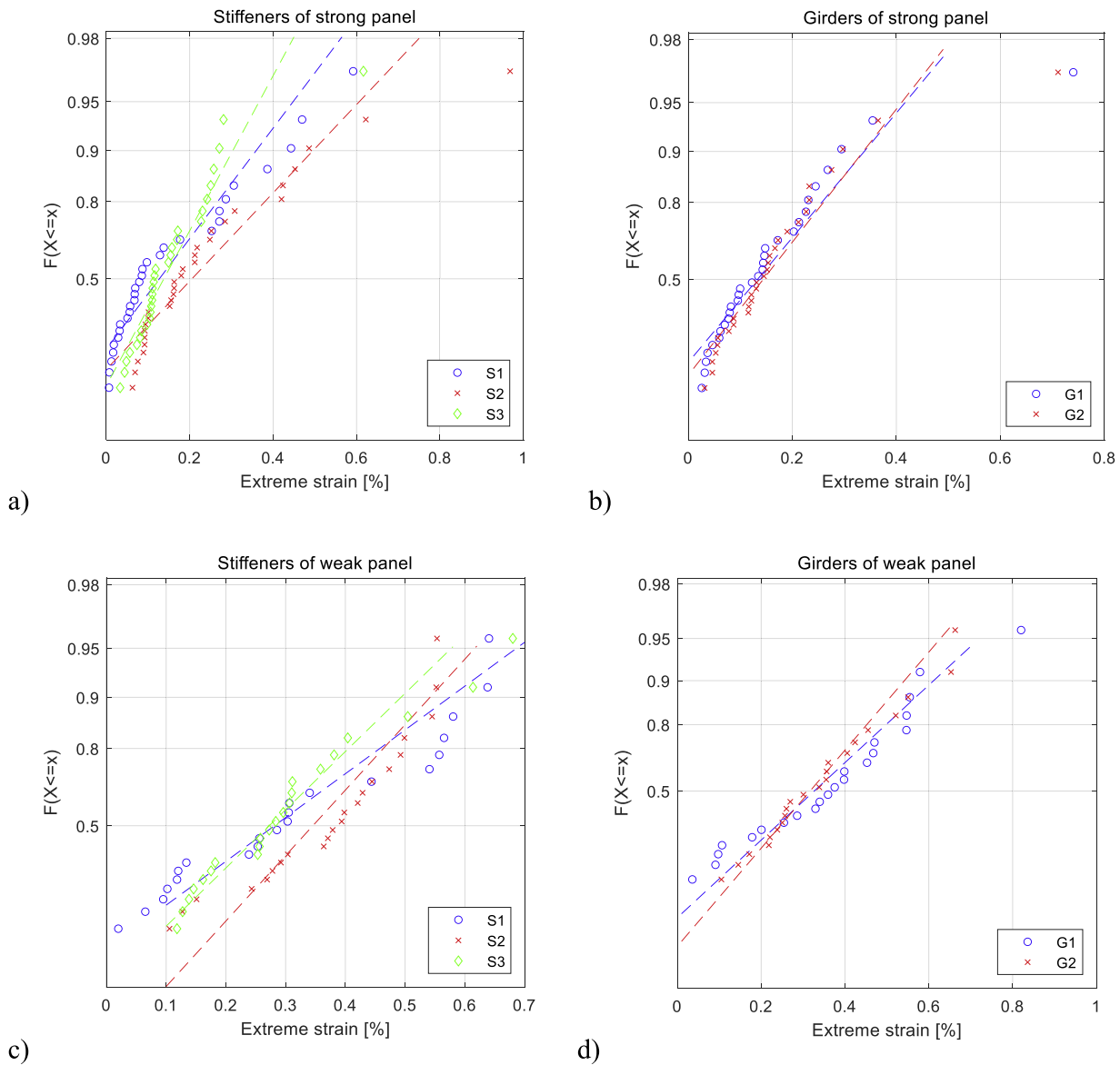


**Fig. 16.** Extreme strains measured inside the elastic panel plotted on Gumbel paper.  $F$  on the y-axis is the probability that the extreme strain  $X$  is lower or equal to the value indicated on the x-axis. Plot a) and b) shows strain on stiffeners and girders of the strong elastic panel and c) and d) shows the strains on the stiffeners and girders of the weak elastic section.

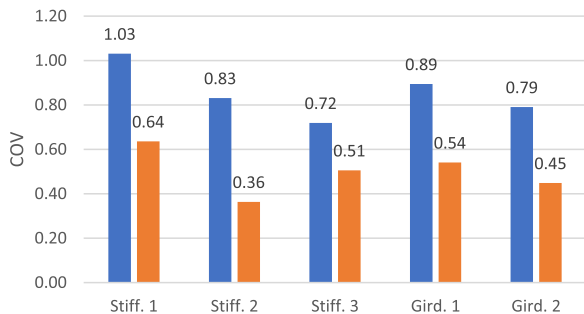


**Fig. 17.** Coefficient of variation of the extreme strains on stiffeners and girders for the strong (blue) and weak (red) elastic sections.

the elastic panel had Young's modulus of 2.7 GPa and Poisson's ratio of 0.39.

(3) The density of the material should have been higher and close to the density of steel. However, since the printed panels were

thicker than what is geometrically scaled thicknesses, the error of the structural mass was lower than the mass error given by the ratio of the model density to steel density. The strong elastic panel were 50 % of the ideal scaled mass and for the weak model panel the mass was 63 % of the ideal scaled mass. This is not believed to be a serious issue since the added mass was found to be roughly 25 times the structural mass.

The lack of geometrical similarity, and differences in material properties makes it hard to relate the strain measurements of the model panel and the full-scale panel by a common factor. However, the objective of the current model test was to obtain validation data, which can be used for statistical comparisons with calculated strains from slamming force measurements using FEA. The validation of these calculations can be carried out considering the elastic model panels. Then afterwards, when the procedure has been validated, the procedure can be applied to real full scale stiffened steel panels.

The combination of 3D printing and advanced material modelling to obtain relevant Froude scaled elastic models has several other relevant

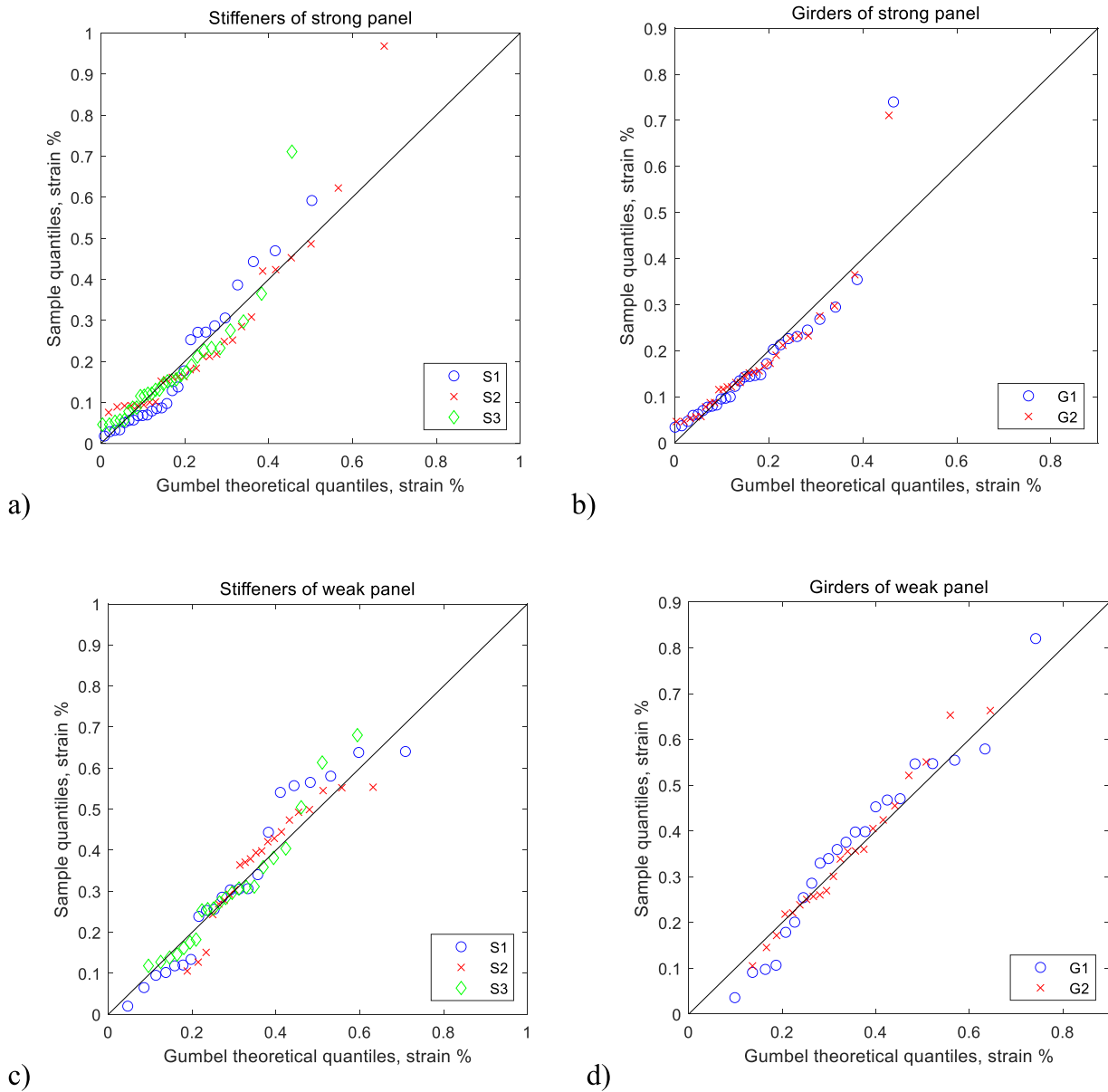


**Fig. 18.** The quantiles calculated from the extreme strain samples as a function of the quantiles estimated from the Gumbel distribution. Plot a) and b) show results for the stiffeners and girders of the strong panel while plot c) and d) show the results the weak panel.

**Table 5**

The measured strains on the strong panel due to static force before and after the completion of the wave impact tests.

Strain point	Load point	Meas. [microstrain] Before	Meas. [microstrain] After	Before-After Deviation
S1	F1	637	634	-0.4%
S2	F3	684	699	2.2%
S3	F5	639	664	3.9%
G1	F2	480	485	1.0%
G2	F4	515	572	11.1%

applications. These techniques are especially relevant for building detailed elastic models in cases where the structure is curved and there is important coupling effects between axial and membrane action. This is the case for shells present in for instance concrete columns (Abrahamsen et al., 2023), closed fish cages or wet decks of catamaran ships.

The time series shows that for all the largest six impacts, for both the

elastic panels, the two girders and the center stiffeners reach positive amplitudes at the same time and that the panels vibrate with close to the same frequency after the time of strain maximum. This suggests that the deformations at these locations are dominated by a global mode of motion with an associated wet natural frequency.

The dry eigenmodes of the strong panel presented in Fig. 15a) shows that the mode associated with the lowest natural frequency is the only out of the first 3 eigenmodes where the strain has the same sign for both girders and the center stiffener. Expressing the response of the panel as a 1 DOF modal system the ratio of the modal added mass to the structural modal mass can be derived as a function of the ratio of the dry to the wet natural frequency. Then using the FE eigenvalue analysis to obtain the dry natural frequency and the measurements to identify the lowest wet natural frequency of the panels the added mass to structural modal mass ratio could be calculated. This 1 DOF model then gives an added mass to structural mass ratio of 25.3 and 26.9 for the strong and the weak panels respectively. The 1 DOF model is simplified, and the added mass was not calculated theoretically. More advanced theoretical estimates of the added mass for the strong elastic panel were carried out by Ahani and

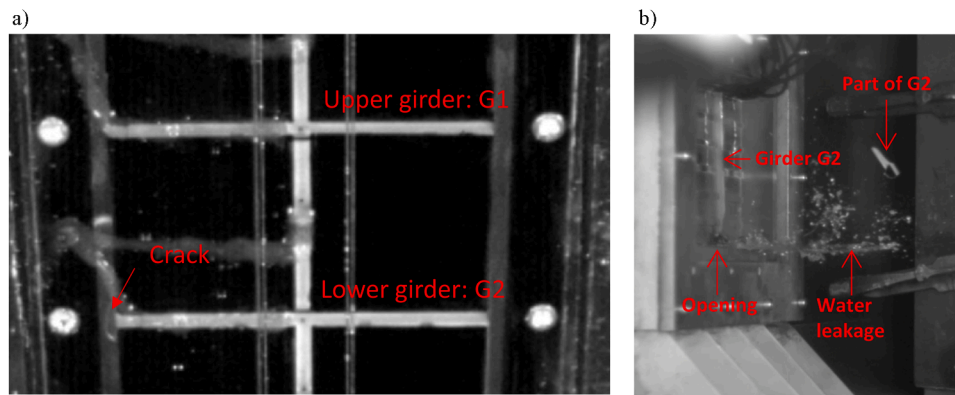


Fig. 19. a) Image from high speed video camera filming the elastic panel from the outside. Image shows a crack developing in the support frame at the intersection with the lower girder G2. b) High speed video frame during the critical wave impact on the weak elastic section filmed vertically downwards into the column showing the dry side of the elastic panel on the left side.

Greco (2023), who analyzed the free vibration problem using a FEM-WAMIT numerical method. A modal method was used expressing the panel deformations as a weighted sum of three dry eigenmodes. In this work the free surface was assumed to be horizontal and the added mass was calculated using Wamit for different submergences of the panel. This theoretical method gave an added mass to structural mass ratio of about 18 when the strong panel was fully submerged. This is lower than the estimate of 25.3 reported herein.

The experimental results show how stiffened panels respond to design critical wave slamming. Engineers designing ocean structures often design the local structure against wave slamming through FE analysis using measured wave slamming forces as input. The accuracy of this and other calculation procedures can be assessed through comparison with the presented results.

The time series show strong decay after the time of maximum strain. Existing hydroelastic theories based on incompressible potential flow theory combined with Wagner theory does not contain any damping terms after the actual impact (Abrahamsen et al., 2023, 2020; Faltinsen, 1999). The structural damping caused by the viscoelastic material behaviour was studied through free decay tests using finite element analysis and contributes to less than 1 % of the damping. The details of the physics causing this fluid mechanic damping is unknown to the authors. However, from a practical engineering point of view, this physics is not necessarily important since the largest strains most often occur during the first half cycle of vibration. For such a short period of time, the damping, if present during this short initial time, would have to be of considerable magnitude to affect the extreme strains.

The extreme value statistics of measured strains are studied and compared to literature on related variables like wave height and local slamming pressures. The hypothesis is that the local structural response is a less sensitive parameter than local slamming pressures. The statistical sensitivity is studied through the coefficient of variation, COV, which is the standard deviation divided by the mean of the sample. Reference COVs are found from Lian (2018) who reports that COVs for extreme slamming loads measured an area of  $3 \times 3 \text{ m}^2$  of a vertical circular cylinder, in comparable wave conditions to ours, were in the range of 0.5 to 1.0 or even higher. As an example of a parameter with low COV is wave crest heights which has COVs in the order of 0.1 see Lian (2018). This difference in COV means that many more realisations of the 3 h wave is required to obtain reliable design values for local slamming pressures than for wave crest heights. For the strong elastic panel, the COVs for the strain responses were in the range from 0.72 to 1.03 and for the weak panel the COV were between 0.36 and 0.64.

The COVs for the strong panel is in the range of COVs for pressures in Lian (2018) case, and hence the uncertainty of the extreme value statistics of strains are in the same order as Lian's pressures for the strong panel. However, since the COV is lower for the weak panel, some

reduced uncertainty of the extreme strains is expected in this case. The reduced COV for the weak elastic panel compared to the strong panel is also consistent with the hypothesis that the structure acts as a filter of the pressure.

The weak panel, having a lower wet natural frequency than the strong panel, filters the loads more efficiently. This filter effect can be realized by looking at classical dynamic amplification factor (DAF) plots of a single degree of freedom mass spring system exposed to a transient load, see Clough and Penzien (1975) p. 94. The DAF is the ratio between the maximum dynamic response to the maximum static response of the system. If the load is of duration less than about  $\frac{1}{4}$  of the natural period, the DAF is proportional to the impulse of the load and not its magnitude. Since the highest slamming loads are associated with the shortest load durations also for wave impact loads (Faltinsen, 1999), it is expected that the structure may act as a filter to these loads provided that the load duration is shorter than  $\frac{1}{4}$ th of the wet natural period.

## 10. Conclusion

The presented hydroelastic wave impact tests provide new understanding of the structural response of stiffened panels during design critical wave slamming. The measurements serve as validation data for FE response calculations from measured slamming pressures. The high-speed videos show that about half of the impacts leading to the largest strains show visible air entrapment / entrainment during the impact. Two stiffened panels were tested, the strong panel had higher stiffeners and girders than the weak panel. The largest measured strain events show that the strain maximum occur nearly simultaneously for the girders and the centre stiffener for both panels. This suggests that the structure responds as a system and not as individual stiffeners and girders alone. The temporal content of the strain time series of critical wave slams shows that the stiffened panels respond with a limited number of wet natural frequencies. For both stiffened panels analysis shows that the added mass associated with the response mode is about 25 times the structural mass. In design of ocean structures, extreme value statistics is important for identifying design responses. The measured extreme strains are compared with the Gumbel distribution. For the strong panel the measured extreme strains are somewhat larger than the strains predicted by the Gumbel model. For the weak panel the Gumbel model fits the measured strains reasonably well. For slamming loads the variability expressed as the coefficient of variation COV may be from 0.5 to 1.0. The present results show that the COVs for the strong elastic panel were of the same order of magnitude as for slamming loads. However, for the weak elastic panel the COV was significantly lower. The reduced COV for the weak compared to the strong panel supports the hypothesis that the structure acts as a filter of the slamming loads.

**CRedit authorship contribution statement**

**Bjørn Christian Abrahamsen:** Supervision, Conceptualization, Resources, Methodology, Software, Validation, Formal analysis, Investigation, Resources, Writing – original draft, Writing – review & editing, Visualization. **Frode Grytten:** Supervision, Conceptualization, Resources. **Erik Andreassen:** Supervision, Conceptualization, Resources. **Øyvind Hellan:** Supervision, Conceptualization, Writing – review & editing.

**Declaration of Competing Interest**

The authors declare that they have no known competing financial interests or personal relationships that could have appeared to influence the work reported in this paper.

**Data availability**

Data will be made available on request.

**Table A1**

The slamming events corresponding to the largest maximum strains measured on top of the stiffeners and girders for the strong panel during all 30 tests.

Rank	Maximum strain at stiffener top.					Time of max  strain					Test number				
	[%]					[s]									
	S1	G1	S2	G2	S3	S1	G1	S2	G2	S3	S1	G1	S2	G2	S3
1	0.592	0.740	0.968	0.711	0.616	9319	5970	5970	5970	5970	30120	30111	30111	30111	30111
2	0.469	0.379	0.622	0.488	0.291	5970	11271	5625	11271	11271	30111	30111	30080	30111	30111
3	0.443	0.354	0.558	0.365	0.281	6685	9319	11271	5625	5625	30100	30120	30111	30080	30080
4	0.386	0.295	0.486	0.297	0.271	6872	2303	9319	9319	8505	30170	30100	30120	30120	30220
5	0.306	0.268	0.452	0.275	0.258	4211	5625	6393	6393	1313	30130	30080	30030	30030	30250
6	0.287	0.245	0.424	0.233	0.250	10700	10700	2303	8505	6135	30290	30290	30100	30220	30140
7	0.271	0.243	0.420	0.233	0.242	11241	6685	3690	3690	9319	30230	30100	30160	30160	30120
8	0.271	0.231	0.308	0.227	0.231	11601	6393	2460	2303	3680	30070	30030	30203	30100	30180
9	0.253	0.226	0.294	0.212	0.227	1836	4211	8152	2460	2303	30280	30130	30120	30203	30100
10	0.230	0.213	0.285	0.190	0.172	2303	11601	8505	4211	2460	30100	30070	30220	30130	30203
11	0.177	0.203	0.252	0.173	0.170	7726	6872	4211	7039	7754	30011	30170	30130	30001	30240
12	0.138	0.172	0.248	0.167	0.157	10872	1836	5696	3835	7039	30011	30280	30001	30011	30001
13	0.138	0.148	0.245	0.156	0.154	2893	8505	6135	7167	9722	30190	30220	30001	30280	30030
14	0.129	0.146	0.218	0.154	0.149	10256	2660	11601	11601	4211	30180	30150	30070	30070	30130
15	0.119	0.144	0.212	0.152	0.147	3591	11241	10700	10700	6393	30120	30230	30290	30290	30030
16	0.114	0.143	0.212	0.147	0.143	5625	2206	11168	5696	5696	30080	30240	30001	30001	30001
17	0.098	0.143	0.212	0.145	0.131	11271	7167	7167	5023	8197	30111	30280	30280	30210	30080
18	0.091	0.135	0.200	0.144	0.118	7633	5696	7039	8197	10700	30170	30001	30001	30080	30290
19	0.087	0.123	0.183	0.134	0.116	6393	10872	5023	6135	9046	30030	30011	30210	30001	30230
20	0.085	0.109	0.182	0.133	0.114	11030	8152	3550	11168	7167	30170	30120	30100	30001	30280
21	0.085	0.104	0.180	0.131	0.111	4829	6135	2660	1313	10829	30210	30001	30150	30250	30150
22	0.081	0.101	0.179	0.131	0.110	3690	3591	8197	6135	6685	30160	30120	30080	30140	30100
23	0.079	0.100	0.177	0.125	0.110	11597	3690	6685	6685	6872	30090	30160	30100	30100	30170
24	0.076	0.097	0.174	0.121	0.110	7039	2893	2257	3680	3835	30001	30190	30130	30180	30011
25	0.073	0.095	0.163	0.121	0.110	2460	10256	6872	6872	11168	30203	30180	30170	30170	30001
26	0.069	0.085	0.163	0.118	0.108	2206	1451	3835	2257	11601	30240	30001	30011	30130	30070
27	0.068	0.082	0.161	0.118	0.108	2660	2087	11241	7956	7956	30150	30060	30230	30220	30220
28	0.068	0.082	0.155	0.116	0.106	8862	7727	2206	2660	5023	30130	30011	30240	30150	30210
29	0.068	0.080	0.152	0.116	0.104	4499	2460	9303	7754	3690	30040	30203	30180	30240	30160
30	0.067	0.079	0.135	0.111	0.099	1345	3550	2598	2206	2660	30180	30100	30120	30240	30150

**Acknowledgments**

This study was supported by Equinor, Aker Solutions, Multiconsult, the Norwegian Shipowners Association and the research council of Norway (RCN) through the SLADE KPN project (RCN Project No. 294748).

**Supplementary materials**

Supplementary material associated with this article can be found, in the online version, at [doi:10.1016/j.apor.2023.103774](https://doi.org/10.1016/j.apor.2023.103774).

**Appendix**

**Table A2**

Largest maximum strain events on the stiffeners and girders during 22 three hour seed variation tests with the weak elastic section.

Rank	Maximum strain at stiffener top.					Time of max  strain					Test number				
	[%]					[s]									
	S1	G1	S2	G2	S3	S1	G1	S2	G2	S3	S1	G1	S2	G2	S3
1	0.640	0.820	0.553	0.663	0.680	2629	7730	7730	8200	8200	40060	40010	40010	40080	40080
2	0.638	0.579	0.552	0.653	0.614	7730	2306	6396	1231	10142	40010	40100	40030	40050	40190
3	0.580	0.555	0.545	0.551	0.505	4214	11604	8200	6396	1231	40130	40070	40080	40030	40050
4	0.565	0.551	0.522	0.521	0.404	2183	1312	1312	7730	7730	40120	40010	40010	40010	40010
5	0.557	0.547	0.499	0.479	0.381	11604	2629	6138	1312	4717	40070	40060	40000	40010	40210
6	0.541	0.547	0.498	0.455	0.358	4832	4214	1454	2306	7042	40210	40130	40000	40100	40000
7	0.503	0.470	0.492	0.424	0.311	4717	6396	1231	10142	6396	40210	40030	40050	40190	40030
8	0.444	0.467	0.473	0.405	0.310	2306	1454	6810	4717	11604	40100	40000	40150	40210	40070
9	0.340	0.453	0.445	0.360	0.306	10332	4717	2306	11604	8572	40111	40210	40100	40070	40200
10	0.309	0.398	0.429	0.356	0.296	7203	4502	3804	7042	2629	40010	40040	40111	40000	40060
11	0.306	0.398	0.421	0.355	0.287	10259	2183	11604	4214	1312	40180	40120	40070	40130	40010
12	0.305	0.388	0.398	0.344	0.284	4502	6138	9752	1454	2306	40040	40000	40090	40000	40100
13	0.303	0.375	0.394	0.339	0.273	1318	5973	4214	3804	4214	40050	40111	40130	40111	40130
14	0.287	0.368	0.379	0.318	0.258	5973	4832	4717	6138	10833	40111	40210	40210	40000	40150
15	0.285	0.359	0.371	0.301	0.256	5772	9419	4502	4502	3804	40080	40050	40040	40040	40111
16	0.256	0.340	0.368	0.270	0.255	7636	10259	8357	2629	3600	40170	40180	40050	40060	40050
17	0.253	0.332	0.364	0.260	0.253	9225	10332	2629	6810	8347	40030	40111	40060	40150	40120
18	0.239	0.330	0.332	0.259	0.251	1454	6810	4832	5973	9584	40000	40150	40210	40111	40000
19	0.234	0.327	0.308	0.257	0.238	1312	5155	5027	9752	1454	40010	40180	40210	40090	40000
20	0.229	0.323	0.304	0.250	0.224	2001	1231	5155	2183	2183	40100	40050	40180	40120	40120
21	0.226	0.301	0.302	0.242	0.214	5824	1318	9419	8357	3922	40180	40050	40050	40050	40010
22	0.211	0.297	0.292	0.239	0.209	11871	7203	11389	9584	4833	40000	40010	40200	40000	40210

**Table A3**  
Extreme strain events on the stiffeners and girders during 30 three hour seed variation tests with the strong elastic section.

Hs 13.3m Tp 13.7s		Extreme strain at stiffener / girder.					Time of extreme strain				
Strong panel		[%]					[s]				
Rank	test no	Stiff 1	Gird 1	Stiff 2	Gird 2	Stiff 3	Stiff 1	Gird 1	Stiff 2	Gird 2	Stiff 3
1	30111	0.47	0.74	0.97	0.71	0.62	5970	5970	5970	5970	5970
2	30080	0.10	0.27	0.62	0.37	0.28	5625	5625	5625	5625	5625
3	30120	0.59	0.35	0.49	0.30	0.24	9319	9319	9319	9319	9319
4	30030	0.09	0.23	0.45	0.28	0.15	6393	6393	6393	6393	9722
5	30100	0.44	0.29	0.42	0.23	0.23	6685	2303	2303	2303	2303
6	30160	0.06	0.10	0.42	0.23	0.10	7189	3690	3690	3690	3690
7	30203	0.03	0.08	0.31	0.21	0.17	2460	2460	2460	2460	2460
8	30220	0.03	0.15	0.28	0.23	0.27	7957	8505	8505	8505	8505
9	30130	0.31	0.23	0.25	0.19	0.15	4211	4211	4211	4211	4211
10	30001	0.03	0.13	0.25	0.17	0.16	7727	5696	5696	7039	7039
11	30070	0.27	0.21	0.22	0.15	0.11	11601	11601	11601	11601	11601
12	30290	0.29	0.24	0.21	0.15	0.12	10700	10700	10700	10700	10700
13	30280	0.25	0.17	0.21	0.16	0.11	1836	1836	7167	7167	7167
14	30210	0.09	0.08	0.18	0.15	0.11	4829	4829	5023	5023	5023
15	30150	0.07	0.15	0.18	0.12	0.11	2660	2660	2660	2660	10829
16	30170	0.39	0.20	0.16	0.12	0.11	6872	6872	6872	6872	6872
17	30011	0.18	0.12	0.16	0.17	0.11	7726	10872	3835	3835	3835
18	30230	0.27	0.14	0.16	0.08	0.12	11241	11241	11241	11241	9046
19	30240	0.07	0.14	0.16	0.12	0.17	2206	2206	2206	7754	7754
20	30180	0.13	0.10	0.15	0.12	0.23	10256	10256	9303	3680	3680
21	30020	0.01	0.03	0.10	0.09	0.06	2550	10360	10360	10360	10360
22	30190	0.14	0.10	0.10	0.09	0.08	2893	2893	2893	2893	10139
23	30040	0.07	0.06	0.09	0.06	0.07	4499	4499	5672	5672	1931
24	30271	0.01	0.04	0.09	0.05	0.10	7889	7889	7889	7889	7889
25	30140	0.02	0.03	0.09	0.13	0.25	6135	6135	6135	6135	6135
26	30250	0.01	0.03	0.09	0.13	0.26	1313	6370	8236	1313	1313
27	30090	0.08	0.07	0.09	0.06	0.05	11597	11597	6109	6109	6109
28	30260	0.06	0.06	0.08	0.05	0.04	2048	6184	6703	6184	6183
29	30050	0.02	0.05	0.07	0.03	0.08	9416	9416	9416	9416	11785
30	30060	0.05	0.08	0.06	0.05	0.03	2087	2087	2087	2087	2087
	Mean	0.15	0.16	0.24	0.17	0.16					
	St. dev.	0.16	0.14	0.20	0.13	0.11					
	COV	1.03	0.89	0.83	0.79	0.72					

Table A4

Extreme strain events on the stiffeners and girders during 22 three hour seed variation tests with the weak elastic section.

Hs 13.3m Tp 13.7s		Extreme strain stiffener / girder.					Time of extreme strain				
Weak panel		[%]					[s]				
Rank	test no	Stiff 1	Gird 1	Stiff 2	Gird 2	Stiff 3	Stiff 1	Gird 1	Stiff 2	Gird 2	Stiff 3
1	40010	0.64	0.82	0.55	0.52	0.40	7730	7730	7730	7730	7730
2	40030	0.25	0.47	0.55	0.55	0.31	9225	6396	6396	6396	6396
3	40080	0.29	0.29	0.55	0.66	0.68	5772	8200	8200	8200	8200
4	40000	0.24	0.47	0.50	0.36	0.36	1454	1454	6138	7042	7042
5	40050	0.30	0.36	0.49	0.65	0.50	1318	9419	1231	1231	1231
6	40150	0.10	0.33	0.47	0.26	0.26	6810	6810	6810	6810	10833
7	40100	0.44	0.58	0.44	0.46	0.28	2306	2306	2306	2306	2306
8	40111	0.34	0.38	0.43	0.34	0.26	10332	5973	3804	3804	3804
9	40070	0.56	0.55	0.42	0.36	0.31	11604	11604	11604	11604	11604
10	40090	0.13	0.18	0.40	0.26	0.12	9111	8779	9752	9752	9752
11	40130	0.58	0.55	0.39	0.36	0.27	4214	4214	4214	4214	4214
12	40210	0.54	0.45	0.38	0.41	0.38	4832	4717	4717	4717	4717
13	40040	0.31	0.40	0.37	0.30	0.18	4502	4502	4502	4502	4502
14	40060	0.64	0.55	0.36	0.27	0.30	2629	2629	2629	2629	2629
15	40180	0.31	0.34	0.30	0.22	0.18	10259	10259	5155	5155	5155
16	40200	0.12	0.25	0.29	0.24	0.31	1390	11389	11389	11389	8572
17	40120	0.57	0.40	0.28	0.25	0.25	2183	2183	2183	2183	8347
18	40170	0.26	0.20	0.27	0.22	0.15	7636	7636	6989	6989	6301
19	40140	0.07	0.09	0.24	0.17	0.16	3057	7235	7235	5241	5241
20	40190	0.10	0.10	0.15	0.42	0.61	2897	2897	10142	10142	10142
21	40161	0.12	0.11	0.13	0.11	0.14	7191	7191	6624	6624	6624
22	40270	0.02	0.04	0.11	0.15	0.13	8432	8432	8432	8432	8432
23	Mean	0.31	0.36	0.37	0.34	0.30					
24	St. dev	0.20	0.19	0.13	0.15	0.15					
25	COV	0.64	0.54	0.36	0.45	0.51					

References

Abrahamsen, B.C., Alsos, H.S., Aune, V., Fagerholt, E., Faltinsen, O.M., Hellan, Ø., 2020a. Hydroplastic response of a square plate due to impact on calm water. *Phys. Fluids* 32, 082103.

Abrahamsen, B.C., Alsos, H.S., Aune, V., Fagerholt, E., Faltinsen, O.M., Hellan, Ø., 2020b. Hydroplastic response of a square plate due to impact on calm water. *Phys. Fluids* 32, 082103.

Abrahamsen, B.C., Grytten, F., Hellan, Ø., Søreide, T.H., Faltinsen, O.M., 2023. Hydroelastic response of concrete shells during impact on calm water. *J. Fluids Struct.* 116, 103804 <https://doi.org/10.1016/j.jfluidstruct.2022.103804>. ISSN 0889-9746.

Ahani, A., Greco, M., 2023. Simplified analysis of wave impacts hydroelastic effects on semisubmersible structure in steel. In: *Proceedings of the International Workshop on Water Waves and Floating Bodies*. USA, 38. IWWWFB.

Bagnold, R.A., 1939. Interim report on wave pressure research. *J. ICE* 12, 201.

Bredmose, H., Bullock, G., Hogg, A., 2015. Violent breaking wave impacts. Part 3. Effects of scale and aeration. *Journal of Fluid Mechanics* 765, 82–113. <https://doi.org/10.1017/jfm.2014.692>.

Clough, R.W., Penzien, J., 1975. *Dynamics of Structures*. McGraw-Hill.

DNV-OTG-14, 2019. Horizontal wave impact loads for column stabilised units.

Faltinsen, O.M., 1999. Water entry of a wedge by hydroelastic orthotropic plate theory. *J. Ship Res.* 43, 180–193.

Faltinsen, O.M., 2006. *Hydrodynamics of High-Speed Marine Vehicles*. Cambridge University Press.

Hattori, M., Arami, A., Yui, T., 1994. Wave impact pressure on vertical walls under breaking waves of various types. *Coast. Eng.* 22 (1–2), 79–114.

Lian G. "Slamming loads on large volume structures from breaking waves", PhD thesis, University of Stavanger, UIS, 2018.

LS-Dyna Finite element software. Livermore Software Technology Corporation. 2023 See <http://www.lstc.com>.

"Materials Data Book". Cambridge University Engineering department, 2003 (online edition).

MSC Nastran 2019 feature pack 1, finite element analysis software.

NORSOK standard N-003, Actions and action effects, 2017.

Okada, S., Sumi, Y., 2000. On the water impact and elastic response of a flat plate at small impact angles. *J. Mar. Sci. Technol.* 5, 31–39.